How are hydrogen bonds modified by metal binding?

Husberg, Charlotte; Ryde, Ulf

Published in:
Journal of Biological Inorganic Chemistry

DOI:
10.1007/s00775-013-0996-2

2013

How are hydrogen bonds modified by metal binding?

Charlotte Husberg, Ulf Ryde *

Department of Theoretical Chemistry, Lund University, Chemical Centre, P. O. Box 124,

SE-221 00 Lund, Sweden

Correspondence to Ulf Ryde, E-mail: Ulf.Ryde@teokem.lu.se,

Tel: +46 – 46 2224502, Fax: +46 – 46 2228648

2014-01-03

Abstract

We have used density-functional theory calculations to investigate how the hydrogen-bond strength is modified when a ligand is bound to a metal, using over 60 model systems involving six metals and eight ligands frequently encountered in metalloproteins. We study how the hydrogen-bond geometry and energy vary with the nature of metal, the oxidation state, the coordination number, the ligand involved in the hydrogen bond, other first-sphere ligands, and different hydrogen-bond probe molecules. The results show that in general, the hydrogen-bond strength is increased for neutral ligands and decreased for negatively charged ligands. The size of the effect is mainly determined by the net charge of the metal complex and all effects are typically decreased when the model is solvated. In water solution, the hydrogen-bond strength can increase by up to 37 kJ/mol for neutral ligands, and that of negatively charged ligands can both increase (for complexes with a negative net charge) or decrease (for positively charged complexes). If the net charge of the complex does not change, there is normally little difference between different metals or different types of complexes. The only exception is observed for sulphur-containing ligands (Met and Cys) and if the ligand is redox active (e.g. high-valent Fe–O complexes).

Key Words: hydrogen bonds, metalloproteins, quantum-mechanical calculations, density-functional theory, dispersion correction, solvation.

Introduction

Hydrogen bonds play an important role in all types of biochemical systems, strongly affecting catalysis, ligand binding, and enzyme function, for example [1]. They have been thoroughly studied by a variety of experimental and theoretical methods [2,3,4,5,6,7,8,9,10, 11,12,13,14,15] so that the strengths of the common hydrogen bonds in biological systems are accurately known.

However, it is well-known that metal sites affect the properties of bound ligands. For example, the pK_a value of water in aqueous metal complexes is reduced from 15.7 for bulk water, to 12.8 for Ca^{2+} and to 2.2 for Fe^{3+} [16]. Therefore, it is also likely that metal ions also change the strength and structure of hydrogen bonds involving their first-sphere ligands. This is of fundamental interest in biological systems, because a great portion of the enzymes contains metal ions in their active sites [17]. Most typical metal ligands in proteins frequently form hydrogen bonds, either directly to the ligating atoms (e.g. Cys, Asp, Glu, Met, and Tyr) or to a neighbouring polar atom in the ligand (e.g. His, Asp, Glu). Non-protein ligands, e.g. from the solvent, can also form hydrogen bonds to the surroundings. These, second-sphere interactions often neutralise the positive charge of the metal ion, e.g. by metal–His–Asp/Glu interactions, or solvate the metal site, e.g. by metal–Cys–HN(backbone) interactions [17,18, 19]. The second-sphere interactions also often modify and tune the properties of the first-sphere ligand. The probably most well-known example of this is push and pull mechanism of haem enzymes, in which the reactivity is changed by varying Fe ligand from His in globins, His–Asp in peroxidases, Cys–HN(backbone) in cytochrome P450, and Tyr–Arg in catalases [20,21,22].

Several studies have shown significant effects of metals. For example, it has been shown that metals in certain cases can be hydrogen-bond acceptors [23,24]. Moreover, the effect of metal ions on water structure has been thoroughly studied by both experimental and theoretical methods [25,26,27,28,29,30]. In particular, there have been several theoretical studies of solvated metal ions, noting that second-sphere water molecules have an increased hydrogen-bond strength [31,32]. Similar studies have also been performed on some models of enzyme catalytic sites [33]. Zarić and coworkers have made a statistical survey of small-molecule crystal structures, which showed that water–water hydrogen bonds become ~0.2 Å shorter and more linear if the donor is coordinated to a metal ion [34]. Moreover, they studied hydrogen bonds between water and a Zn^{2+} complex and showed that the hydrogen-bond strength increased from 20 kJ/mol for free water, via 23 kJ/mol for the neutral $ZnCl_2(H_2O)_4$ complex to 92 kJ/mol for the doubly charged $[Zn(H_2O)_6]^{2+}$ complex. Schmiedekamp and Nanda have shown that both NH–OH_2 and CH–OH_2 hydrogen bonds from His residues become much stronger if the His residue coordinates to Zn^{2+} or $Fe^{2+/3+}$ [35]. For example, the NH–OH_2 bond strength increased from 28 kJ/mol for free imidazole to 69 and 105 kJ/mol for $Fe(NH_3)_5$(imidazole) in the Fe^{2+} and Fe^{3+} states, respectively. A similar increase in the hydrogen-bond strength of iron-coordinated His residues has also been observed for the active site of haemerythrin [36]. The hydrogen-bond strength of O_2 and CO to a histidine residue has also been shown to increase when they bind to Fe in haem proteins [37].

All these studies have been restricted to only a few metals and ligands. In this paper, we make a more systematic study of how metal ions affect the strength and structure of hydrogen bonds to their first-sphere ligands. The study employs accurate dispersion-corrected density-functional theory (DFT) calculations. We study how the hydrogen-bond strength depends on the type of metal and its oxidation state, the coordination number, the type of the ligand, other ligands of the metal, and on the nature of the second-sphere hydrogen-bond partner. We study over 60 different complexes, taken mainly from our previous theoretical studies of various metalloproteins [18,19,22,38,39,40,41,42,43,44,45,46,47]. The results provide much insight into how metal coordination affects the geometry and energy of hydrogen bonds to ligating

amino-acid residues.

Methods

All geometry optimisations were performed with the Becke-1988–Perdew-1986 DFT functional (BP86) [48,49]. They employed the DZP basis set for the metal ions and 6-31G* for all other atoms, but we included diffuse functions (6-31+G*) on the hydrogen-bond donor and acceptor atoms, and a polarising function for the hydrogen-bond hydrogen atom (6-31G**) [50,51,52]. The calculations were sped up by expansion of the Coulomb interactions in auxiliary basis sets, the resolution-of-identity approximation[53,54].

For each optimised structure, a frequency calculation was performed at the same level of theory to ensure that a proper stationary structure or saddle point was obtained. These frequency calculations also permitted calculation of zero-point vibrational energies and thermal corrections to the enthalpy, obtained by a rigid-rotor harmonic-oscillator ideal-gas approximation at 298 K and 1 atm pressure. More accurate single-point energies were also calculated on these structures using the hybrid B3LYP functional [55,56] and the 6-311+G(3d,2p) basis set on all atoms [52].

Environmental effects were incorporated by single-point calculations in a continuum solvent with different dielectric constants, $\varepsilon = 4$ or 80, using the Cosmo approach with optimised radii and 2.0 Å for the metals [57,58,59]. These calculations were performed with the same method as for the geometry optimisations. Together with the vacuum results ($\varepsilon = 1$), they should include possible effects in a protein, for which the dielectric constant is usually assumed to be between 2 and 20 [60,61]. The QM calculations were performed with the Turbomole software [62].

Dispersion effects were calculated by single-point calculations using the DFT-D3 method [63], as calculated with the dftd3 program for the B3LYP level with default parameters [64]. In addition, continuum estimates of the cavitation, dispersion, and repulsion energies for all complexes with the surroundings were estimated with the polarised continuum method (PCM) [65,66], as implemented in the Gaussian03 software [67]. These calculations used the UAKS radii (united atom topological model for Kohn–Sham theory). The non-polar solvation energies are needed to obtain a balance in the solvation and dispersion energy terms for these reactions involving the formation of a new hydrogen bond from two isolated molecules [68].

Finally, corrections to the basis-set superposition error were estimated using the counter-poise method [69] at the B3LYP/6-311+G(2d,2p) level of theory. To simplify comparison with previous studies of hydrogen bonds [10,11,12,13,14] and to obtain the most stable results, we present in the main article pure hydrogen-bond energies at the B3LYP/6-311+G(2d,2p) level of theory (the energy of the complex minus the energy of the two monomers, all at optimised geometries) and they include counter-poise corrections (the energy difference of each monomer calculated with the complex and monomer basis set at the complex geometry) and DFT-D3 dispersion, but no other corrections. Results are given for three values of the dielectric constant (1, 4, and 80). These energies are close to reference coupled-cluster results (CCSD(T)) with complete basis-set extrapolations [10,11,12,13,14]. For example, we obtain in vacuum a hydrogen-bond energy of 19 kJ/mol for the water dimer, which is only 2 kJ/mol lower than the reference value of 21 kJ/mol [13]. Likewise, our hydrogen-bond energy for the $CH_3CONHCH_3$–HOH complex, 34 kJ/mol is identical to the S66 reference value [13]. The raw BP86 results, counter-poise corrections, geometry relaxation energies, DFT-D3 dispersion energies, PCM solvation effects, the zero-point energy and thermal corrections to the enthalpy and entropy are listed in Tables S1–S9 in the supporting information. For convenience, we will throughout this paper discuss hydrogen-bond energies as positive entities, i.e. the negative of the energy of formation of the hydrogen bond.

Results

In this article, we have studied how metal ions affect the hydrogen-bond strength of their first-sphere ligands. We have studied over 60 different metal complexes of nine different types, as well as the corresponding hydrogen bonds in the absence of the metal ion. We study the hydrogen bond by adding a probe molecule to the metal complex, typically water, but sometimes instead imidazole or acetate. In this section, we will describe the results for each type of complex in separate sections. In the next section, we will discuss general results and trends over all types of complexes.

Protonated compound II models with different axial ligands

We first studied a series of five models of protonated compound II with different axial ligands [22]. All models contained a Fe ion in the formal +IV oxidation state, in the centre of a porphine ring (i.e. a haem group without any peripheral ligands). One axial ligand was OH^-, whereas the other axial ligand was varied, CH_3S^- as a model of Cys in cytochrome P450, imidazole as a model of His in globins, imidazole hydrogen-bonded to an acetate group as a model of His+Asp in peroxidases, and phenolate with or without a hydrogen-bonded guanidine group, as a model of the Tyr(+Arg) ligand in catalases. To all models, a water probe molecule was hydrogen bonded to the OH^- group with the water molecule as the donor (i.e. with a HO–HOH pattern). The five models are shown in Figure 1. Following previous theoretical and experimental experience [22], all models were studied in the intermediate-spin triplet state. The His and Tyr+Arg complexes had a +1 net charge, whereas the other three models were neutral. This protonated compound II state (formally Fe^{IV}–OH^-) has been suggested in the reaction mechanism of many haem oxidases, although the current consensus is that it is only involved in the reaction mechanisms when the axial ligand is Cys (the intermediate between the hydrogen-atom transfer and the rebound steps of cytochrome P450) [70,71].

In the absence of the metal ion, a $^-$HO–HOH hydrogen bond is strong, owing to the negative charge of the hydroxide ion, with a hydrogen-bond O–H distance (the distance between the O atom of the OH^- ligand and one of the H atoms of the water probe) of 1.23 Å and a hydrogen-bond strength of 117 kJ/mol in vacuum, which is strongly reduced to 31 kJ/mol in continuum water solution.

This strength is strongly reduced when OH^- is bound to the metal. The O–H hydrogen-bond distance increases to 1.79–1.85 Å for all axial ligands and the bond strength decreases to 26–38 kJ/mol in vacuum as can be seen in Table 1. The bond is shortest and strongest for the three neutral complexes and weaker for the two positively charged complexes. The hydrogen bond is also 4–8 kJ/mol weaker for complexes with His than for the other complexes with the same net charge. The hydrogen bond to water always makes the Fe–OH^- bond length longer by ~0.02 Å and shortens the bond length to the axial ligand by 0.01–0.07 Å (most for His).

The protonated compound II is formally a Fe^{IV}–OH^- state and the electronic structure is close to this description with 1.6–2.1 unpaired electrons on Fe (most for Tyr+Arg and least for Tyr) and 0.1–0.2 unpaired electrons on OH^- , 0.2 electrons in the porphine ring (0–0.1 *e* for His), 0–0.5 spins on the axial ligands (the least for His and Tyr+Arg, and most for Tyr), but no spin on the second-sphere ligand or the water probe. The water hydrogen bond consistently increases the spin density on OH^-, but only by ~0.04 *e*.

Cytochrome models

The second set of calculations was performed on six cytochrome models with three different metal ions (Fe, Co, and Ni) in two oxidation states (+II and +III). The models

contained the metal ion in the centre of a porphine ring and with two imidazole groups as axial ligands. A water probe was bound to the non-coordinating N atom of one of the imidazole groups by a NH–OH_2 hydrogen bond as can be seen in Figure 2. Following our previous studies [45,46], all complexes were studied in the low-spin states, except Ni^{III}, which was studied in the triplet state.

Without the metal, the imidazole–water NH–OH_2 hydrogen bond is rather weak, with a H–O bond length of 1.97 Å and a strength that goes from 23 kJ/mol in vacuum to 8 kJ/mol in water solvent, as can be seen in Table 2.

The +2 metal ions, which give rise to neutral complexes (the porphine ring has a double negative charge), barely change the hydrogen-bond strength: The H–O bond length decreases to 1.90–1.95 Å and the hydrogen-bond energy increases by 0–3 kJ/mol. With the +3 metal ions, the hydrogen bond is shortened to 1.84–1.86 Å. The strength increases to 39–41 kJ/mol in vacuum, but in water solution all complexes give hydrogen bonds that are not more than 2 kJ/mol stronger than that of free imidazole. This indicates that the increased bond strength is mainly caused by the extra positive charge of the complexes with the trivalent metal ions. The hydrogen-bond energies show the trends $Fe^{2+} > Ni^{2+} > Co^{2+}$ and $Fe^{3+} > Co^{3+} > Ni^{3+}$, but the differences are small (3 kJ/mol) and the trends are blurred when solvation effects are included.

Peroxidase models

In the third set of models, we kept iron as the metal and imidazole as one of the axial ligands (and porphine as the haem model). Then we varied the oxidation state of the metal ion and the protonation state of the other, water-derived, axial ligand. In addition, we used two different hydrogen-bond probe molecules, water or imidazole (as a model of the distal His residue in globins or peroxidases).

With imidazole as the probe, we kept the metal at the formal Fe^{IV} state and studied the three possible protonation states of the water ligand, H_2O, OH^-, and O^{2-}. H_2O must be a donor and therefore forms HOH–N hydrogen bonds. In the globins, this corresponds to a state with the distal His protonated on the ND1 atom, and we will call such a state HID in the following [41]. Likewise, O^{2-} is always an acceptor, forming O–HN hydrogen bonds, but we tested both neutral imidazole and the positive imidazolium ion as the donor. We will call these two states HIE and HIP in the following. OH^- can be both a hydrogen-bond donor and an acceptor (to both imidazole and imidazolium) and we tested all three possibilities, giving a total of six different states.

With water as the hydrogen-bond probe, we studied the same Fe^{IV} states, with water both as the donor and acceptor for with the OH^- ligand. In addition, we studied with the OH^- ligand as the acceptor also three additional formal oxidation states of the metal, Fe^{II}, Fe^{III}, and Fe^{V}. Finally, we studied for the Fe^{IV}–H_2O state also a hydrogen bond to the non-coordinating N atom of the imidazole ligand. This gave a total of eleven types of complexes, which are shown in Figure 3. Following previous calculations [22,40,41,42], all Fe^{IV} complexes were studied in the intermediate-spin triplet state, whereas the other three oxidation states were studied in the low-spin state (singlet for Fe^{II} and doublet for Fe^{III} and Fe^{IV}).

We start to discuss the four complexes with OH^- as the axial ligand, water as the probe, and the Fe ion in different oxidation states. All four complexes form the same HO–HOH hydrogen bond, which also was studied in the protonated compound II series. We saw above that the isolated OH^- ion gave a very strong hydrogen bond with an O–H distance of 1.23 Å and a bond energy of 117 kJ/mol. All the metal complexes give appreciably weaker hydrogen bonds, following the oxidation state ($Fe^{II} > Fe^{III} > Fe^{IV} > Fe^{V}$): 1.63, 1.76, 1.85, and 1.94 Å for the O–H distance, and 84, 44, 26, and 35 for the binding energy, respectively, as can be seen

in Table 3. This trend follows also the net charge of the complex (–1 to +2), showing that the effect comes mainly from neutralisation of the negative charge of the OH^- ion. The trend remains in water solution, in which the hydrogen-bond energies are 50, 25, 3, and 2 kJ/mol.

For the Fe^{IV}–OH^- state we tested also OH^- as the hydrogen-bond donor, i.e. an $OH–OH_2$ pattern. Interestingly, this gave a stronger complex than the one with the opposite (HO–HOH) pattern, with a H–O distance of 1.71 Å and an energy of 44 kJ/mol, 18 kJ/mol stronger than the other pattern. This is quite surprising considering that the isolated OH^- ion is a poor hydrogen-bond donor and no $^-OH–OH_2$ complex can be found for the isolated system. Apparently, metal coordination changes this pattern completely.

Next, we compare the three protonation states of the water-derived ligand, keeping the metal ion in the formal Fe^{IV} oxidation state, still with the water probe. The Fe^{IV}–H_2O complex forms a strong hydrogen bond to water with a H–O distance of 1.60 Å and a hydrogen-bond energy of 76 kJ/mol. This is appreciably stronger than for the isolated $HOH–OH_2$ complex, which has a H–O distance of 1.91 Å and an energy of 19 kJ/mol. In water solution, the difference has been reduced to 20 kJ/mol.

For this complex, we also tested the strength of a hydrogen bond the axial imidazole group. This imidazole $NH–OH_2$ interaction is slightly weaker, 1.73 Å and 60 kJ/mol. Still, this is appreciably stronger than the corresponding complex without the metal, 1.97 Å and 23 kJ/mol. However, in water solution, the isolated complex is only 1 kJ/mol weaker, showing that the effect comes mainly from the +2 net charge of the Fe^{IV}–H_2O complex. It is notable that metal coordination changes the relative stabilities of the water–imidazole and water–water hydrogen bonds, most likely because the water oxygen atom is the metal ligand, whereas in imidazole, the hydrogen bond is not to the coordinating atom, reducing the effect of metal coordination.

Next, we studied also the Fe^{IV}–O^{2-} complex. It gave a rather weak O–HOH bond of 1.82 Å and 34 kJ/mol. This is much weaker than the isolated $^{-2}O–HOH$ complex, with an O–H distance of 1.51 Å and an energy of 177 kJ/mol (this complex can be obtained only with fixed water H–O bonds). The difference is mainly caused by the difference in net charge between the two systems (0 and –2) and it is inverted in water solution.

Finally, we studied the same three protonation states of the water-derived ligand bound to Fe^{IV}, but using instead imidazole or the imidazolium cation as the probe. For the Fe^{IV}–H_2O complex, a strong HOH–N hydrogen bond of 1.59 Å was obtained (but only with a fixed O–H bond; otherwise the proton is transferred, giving rise to the Fe^{IV}–HO–imidazolium complex, discussed below). This distance is similar to the one found for with the water probe, but the energy is much larger, 142 kJ/mol, compared to 76 kJ/mol. The difference is still 29 kJ/mol in water solution. This complex is also much stronger than the isolated imidazole–HOH complex, which has a N–H distance of 1.87 Å and an energy of 32 kJ/mol.

For the Fe^{IV}–OH^- model, we studied three different hydrogen-bonded complexes, two with imidazole, either as acceptor (HID) or donor (HIE), and one with the imidazolium cation as a donor (HIP). The HID state gave a very strong OH–N bond of 1.39 Å and with an energy of 85 kJ/mol. Again, no such complex with OH^- as the hydrogen-bond donor could be found in isolation.

The HIE complex with the opposite HO–HN pattern was 28 kJ/mol less stable than the HID state, as is also illustrated by the much longer O–H distance, 1.75 Å. The hydrogen-bond energy, 58 kJ/mol, is much smaller than for the corresponding isolated imidazole–OH^- complex, 171 kJ/mol, which has an O–H distance of 1.48 Å (obtained with a N–H distance constraint). However, in water solution, the difference is only 11 kJ/mol.

Interestingly, the HIP complex, shows an unfavourable binding energy of 55 kJ/mol, although the O–H hydrogen-bond distance is short, 1.52 Å. The reason for this is that it is obtained from two moieties with the same +1 net charge, leading to a strong Coulombic

repulsion. This is overcome in water solution, where a favourable binding energy of 34 kJ/mol is obtained. However, the corresponding free $^{-}$HO–imidazolium^{+} complex, formed from two oppositely charged moieties, is much stronger even in water solution (65 kJ/mol; 1.26 Å distance, obtained with N–H fixed).

Finally, we studied also two Fe^{IV}–O^{2-} complexes, one with imidazole (HIE) and the other with imidazolium (HIP) as the hydrogen-bond donor. The former complex forms a rather weak hydrogen bond with an O–H distance of 1.80 Å an energy of 53 kJ/mol. This is much weaker than the free imidazole–O^{2-} complex (1.34 Å and 189 kJ/mol), but this trend is reversed already with a dielectric constant of 4 (because the metal complex is neutral and therefore little affected by solvation).

The Fe^{IV}–O HIP complex is tautomeric to the Fe^{IV}–OH HID state and the two states are close in energy (the latter state is 2 kJ/mol more stable in vacuum, but 2 kJ/mol less stable in water solution). The Fe^{IV}–O HIP state has a strong hydrogen bond with an O–H distance of 1.26 Å and a bond energy of 187 kJ/mol, which is reduced to 28 kJ/mol in water solution. As expected, this is weaker than for the free imidazolium^{+}–O^{2-} complex in vacuum (1.07 Å and 1103 kJ/mol), but it is stronger in water solution.

Superoxide dismutase models

Next, we studied twelve models of Fe and Mn superoxide dismutase. We studied three types of models with an increasing number of ligand. The first was a five-coordinate structure in which the metal binds to three imidazole groups (models of His ligands) and one bidentate acetate group (as a model of the Asp ligand). In the second type, a water ligand was added, which replaced one of the acetate oxygen atoms as the fifth ligand of the metal. In the third type, we added a superoxide molecule as a sixth ligand of the metal. In all cases, we used a water probe, forming a hydrogen bond to the imidazole group that was not trans to another imidazole group, with a NH–OH_2 pattern. The three types of complexes are shown in Figure 4. All three types of complexes were studied for both Fe and Mn, and with these two metals in the formal oxidation states of +II and +III, giving twelve complexes in total.

With four and five ligands, the complexes were studied in the high-spin state [47]. The electronic structure was also close to the expected +II and +III metal states, with only minor spin on the imidazole, acetate, and water ligands (less than 0.1 *e*) and no spin on the hydrogen-bonding water probe, as can be seen in Table 4. The only exception was Fe^{3+}, which showed a larger spin delocalisation onto the ligands, up to 0.3 *e* on the acetate group. However, for the complexes with superoxide, the unpaired spin on the latter ligand mixes with the spins on the metals. Following our previous studies [47], the Fe complexes had one extra unpaired electron. For the two M^{2+} complexes, the electronic structures were similar to those of the five-coordinate complexes, but with an extra aligned spin on superoxide. For Fe^{3+}, the superoxide had instead 1.65 unpaired electrons, i.e. closer to a peroxide ion, and this electron was taken mainly form the iron ion. For the Mn^{3+} complexes, the spin on superoxide was instead antiferromagnetically coupled to that on Mn, which gave a mixed electronic structure with 1.4 unpaired electrons on O_2.

The geometries of the optimised complexes are described in Table 4. The structures are similar to those found in our previous study [47], so they will not be further discussed. The NH–OH_2 hydrogen-bond distance is 1.67–1.94 Å, i.e. somewhat shorter than for the free imidazole–water complex (1.97 Å). It is always shorter for the +3 ions (1.67–1.84 Å) than for the +2 ions (1.82–1.94 Å) and also shorter in the five-coordinate complexes than in the six-coordinate complexes, mainly because of the extra positive charge in the former (+1 or +2), compensated by the single negative charge on the superoxide ligand in the latter. The bond is also shorter for Mn than for Fe, but the difference is less than 0.03 Å and often minimal.

The hydrogen-bond strength shows similar trends: In vacuum, it is always stronger than for free imidazole (26–70 kJ/mol compared to 19 kJ/mol). It is always stronger for the +3 ions (42–70 kJ/mol) than for the +2 ions (26–44 kJ/mol) and it is stronger for the five-coordinate complexes than for the six-coordinate complexes. Mn has often a slightly stronger bond than Fe, but not always. In continuum-water solution, most of these differences have disappeared, and all complexes have the same hydrogen-bond strength within 6 kJ/mol (7–13 kJ/mol), i.e. slightly stronger than that of free imidazole (4 kJ/mol).

MS_4 clusters

Next, we studied two models with a metal ion surrounded with four Cys ligands, modelled as $[M(CH_3S)_4]^{2-}$ with either Fe^{2+} or Zn^{2+} as the central metal. These are models of the iron–sulphur cluster in rubredoxin or a structural zinc ion, e.g. in zinc fingers or in alcohol dehydrogenase [17,19,21]. In variance to sites with many His ligands, the net charge of these metal sites is not compensated by second-sphere charged groups, but instead by an extensive solvation by neutral backbone groups or water molecules. We therefore probed the strength of hydrogen bonds from a water molecule to the ligating Cys atoms. Fe^{2+} was studied in the high-spin quintet state, whereas Zn^{2+} was a closed-shell singlet.

For Fe^{2+} we studied complexes with the water molecule forming hydrogen bonds to either one or two sulphur ligands (cf. Figure 5). The results in Table 5 shows that for the former, the S–H distance was 2.19 Å and the hydrogen-bond energy was 68 kJ/mol, which decreased to 9 kJ/mol in water solution.

Interestingly, if the water molecule forms two hydrogen bonds, both bonds become quite weak with S–H distances of 2.35 and 2.44 Å. Moreover, the bond energy increases by only 4 kJ/mol compared to the complex with a single hydrogen bond, i.e. to 72 kJ/mol. However, the energy is less affected by solvation and the difference increases to 10 kJ/mol in water solution.

For Zn^{2+}, we only studied the complex with two hydrogen bonds. It turned out that water formed somewhat stronger hydrogen bonds to the Zn^{2+} complex than to the Fe^{2+} complex, with S–H distances of 2.32 and 2.41 Å and a 12 kJ/mol larger hydrogen-bond energy of 84 kJ/mol in vacuum. The difference decreased to 5 kJ/mol in water solution. The reason for the stronger hydrogen bonds of the Zn^{2+} complex may be that significant spin is delocalised on each of the Cys ligands (~0.1 *e*) in the Fe^{2+}, although the Mulliken charges are larger on the sulphur atoms in the Fe^{2+} complex (–0.9 *e* compared to –0.8 *e*). All hydrogen bonds were longer than that of the isolated $^{-}CH_3S$–HOH complex (2.15 Å), but the hydrogen-bond energies were similar (66 kJ/mol in vacuum and 15 kJ/mol in water solution).

Carboxypeptidase models

We also studied three models of the active site in carboxypeptidase, i.e. a Zn^{2+} ion with one water, one Glu (modelled by an acetate ion), and two His ligands (modelled by imidazole). With a water molecule, we probed the hydrogen-bond strength to each of the three types of ligands as is shown in Figure 6.

First, we studied a HOH–OH_2 hydrogen bond to the water ligand. As can be seen in Table 6, it was quite short, 1.74 Å and rather strong, 46 kJ/mol. This is appreciably shorter and stronger than the free HOH–OH_2 complex (1.91 Å and 19 kJ/mol). The difference remained in water solution, but it was decreased to 12 kJ/mol.

A hydrogen bond to the non-coordinating nitrogen atom of the imidazole model was somewhat longer (1.80 Å H–O distance), but slightly stronger 47 kJ/mol, although the difference was reversed in water solution. This is appreciably stronger than for a free

imidazole–OH_2 complex (1.97 Å and 23 kJ/mol), but the difference almost disappears in water solution.

Interestingly, a hydrogen bond to the carboxylate ligand is slightly longer, with an O–H distance of 1.81 Å, although the hydrogen-bond energy was slightly larger, 50 kJ/mol. This is appreciably weaker than for the free acetate–HOH complex, even in this less stable anti configuration, with a 1.57 Å O–H distance and bond energy of 70 kJ/mol. The difference remains in water solution.

Azurin models

Next, we studied a series of ten models of the active site in the blue-copper protein azurin. It contains a copper ion, coordinated to three strong ligands from one Cys and two His residues (modelled by CH_3S^- and imidazole). In addition, there are two weaker ligands from a backbone carbonyl group (covalently connected to one of the His ligands and therefore modelled by $CH_3CONHCH_2CH_2$–imidazole) and the side chain of a Met residue (modelled by CH_3SCH_3), forming a trigonal bipyramidal geometry. The bond distances to the latter two ligands are strongly affected by the surrounding protein [38], so we constrained them to the distance found in crystal structures [72,73]. We have studied this site in both the reduced Cu^+ (closed-shell singlets) and the oxidised Cu^{2+} states (doublet), and we have measured the strength of hydrogen bonds between a probe water molecule and each of the five ligands, i.e. to the coordinating S atoms of the Cys and Met ligands (S–HOH bonds), the coordinating O atom of the backbone model (O–HOH), and to the non-coordinating N atoms of imidazole models (NH–OH_2 bonds). The five different types of hydrogen bonds are shown in Figure 7.

The results of these calculations are collected in Table 7. For the reduced complex, the hydrogen bonds to the His ligands are rather weak with H–O bond lengths of 1.93–1.94 Å and bond energies of 26–27 kJ/mol. The bond length is slightly shorter than for the free imidazole–OH_2 complex (1.97 Å) and the bond energy is slightly larger (23 kJ/mol). For the oxidised models, the hydrogen bonds are stronger with a NH–O distance of 1.85 Å and bond energies of 40–41 kJ/mol. In water solution, the bond energy is ~9 kJ/mol for both the reduced and oxidised complexes, which is 1 kJ/mol stronger than for the free complex.

The reduced complex shows a quite strong hydrogen bond to the Cys ligand with a S–H distance of 2.14 Å, which is almost the same as for the free $^-CH_3S$–HOH complex (2.15 Å). However, the hydrogen-bond energy is appreciably lower, 46 kJ/mol, compared to 66 kJ/mol for the free complex, reflecting that the azurin complex is neutral, whereas the free complex is negatively charged. Consequently, the difference disappears in solution and in water solvent, the azurin model has the stronger bond by 10 kJ/mol.

Interestingly, the hydrogen bond to the Cys ligand in the oxidised complex becomes appreciably weaker, in spite of the change of the net charge to +1: the S–H distance increases to 2.44 Å and the bond energy decreases to 25 kJ/mol. The reason for this is that the unpaired electron is shared between the copper ion and the Cys ligand in the oxidised state: The spin densities of these two groups are 0.39 and 0.48 *e* (0.33 and 0.57 *e* without the water probe or with the probe binding to the other ligands), showing that the ligand is partly a neutral $CH_3S^\bullet$ radical.

The Met ligand forms an unexpectedly strong hydrogen bond in the reduced complex with a S–H distance of 2.23 Å and a bond energy of 35 kJ/mol. This is much stronger than for the free $(CH_3)_2S$–HOH complex, which has a S–H distance of 2.43 Å and a bond energy of 18 kJ/mol. However, the difference is reversed in water solution. In the oxidised complex, the S–H bond becomes longer, 2.37 Å and the hydrogen-bond energy decreases by 1 kJ/mol.

The hydrogen bond to the backbone carbonyl group is rather strong in the oxidised complex. The O–H distance is 1.74 Å, slightly shorter than in the free $CH_3CONHCH_3$–HOH

complex (1.80 Å). The hydrogen-bond energy is 4 kJ/mol larger in the complex. For the reduced model, we have not been able to obtain a pure hydrogen bond to the carbonyl group, but instead it also forms a hydrogen bond to the Cys ligand (even if started from the structure of the oxidised state), making the structure (a H–S distance of 2.36 Å and a H–O distance of 2.01 Å) and the hydrogen-bond energy (54 kJ/mol) harder to interpret.

Nitrite reductase models

We have also studied five models of the active Cu^{2+} site of nitrite reductase. In the resting form, the copper ion is in the oxidised state with three His ligands and a solvent molecule. Previous calculations have shown that the solvent molecule can be either water or OH^- [20]. Therefore, we have studied complexes with these two ligands, hydrogen-bonded to a water probe (for OH^- with the probe either as a donor and an acceptor). In the enzyme, this group instead forms a hydrogen bond to a carboxylate group. Therefore, we have also used acetate (Ac^-) as a probe. The calculation was started with a H_2O ligand, but during the geometry optimisation, a proton moved from the ligand to the acetate group, forming a HO–HAc pattern. In the enzyme, another carboxylate group forms a hydrogen bond to one of the His ligands. Therefore, we have also studied such an interaction. Structures of all five complexes studied are shown in Figure 8. All complexes were studied in the doublet Cu^{2+} state.

The results are collected in Table 8. The Cu–ligand distances strongly depend on the nature of the fourth ligand. If it is water, the Cu–O distance is long and flexible (2.07–2.36 Å), and the distances to the imidazole ligands are short, ~1.98 Å on average. If the ligand instead is OH^-, the Cu–O distance is short, 1.89–1.91 Å, and the distances to the imidazole ligands are somewhat longer, ~2.03 Å on average. Hydrogen bonding to the water ligand makes the Cu–O bond appreciably shorter (2.07 compared to 2.18 Å), whereas it becomes slightly longer for the OH^- ligand (by up to 0.02 Å). Binding of acetate to one of the His ligands makes the corresponding Cu–N bond 0.01 Å shorter, but at the same time the Cu–N bond to the cis His and water ligands became 0.10 and 0.16 Å longer.

Water forms a quite strong hydrogen bond to the water ligand, with a H–O distance of 1.60 Å and a hydrogen-bond energy of 76 kJ/mol. This is appreciably stronger than for the corresponding free $HOH–OH_2$ complex (1.91 Å and 19 kJ/mol). This difference decreases to 4 kJ/mol in water solution.

Interestingly, hydrogen bonds to the OH^- ligand are weaker. For this nitrite-reductase model, OH^- forms stronger hydrogen bonds as an acceptor than as a donor: The O–H distance is 1.70 Å compared to 1.80 Å, and the hydrogen-bond energy is 40 compared to 15 kJ/mol. However, the acceptor complex is still much weaker than the free $^-HO–HOH$ complex (1.23 Å and 117 kJ/mol), a difference that remains also in water solution.

The acetic-acid group gives a rather strong hydrogen bond to the OH^- complex, with an O–H distance of 1.57 Å and an energy of 69 kJ/mol. However, both the distance and the energy are more similar to that of a free $^-Ac–HOH$ complex (1.57 Å and 70 kJ/mol) than to the $HAc–OH^-$ complex (1.36 Å and 171 kJ/mol).

The binding of an acetate group to an imidazole ligand of the water complex gives a rather short hydrogen bond of 1.62 Å. However, the bond energy is very high (667 kJ/mol) owing to the binding of a negatively charged ligand to a copper complex with a double positive charge. Consequently, the energy is much reduced by solvation and becomes strongly unfavourable (by 64 kJ/mol) in water solution. The corresponding free imidazole–Ac^- complex has a slightly shorter H–O bond (1.54 Å), but a much smaller bond energy (121 kJ/mol; because the imidazole group is neutral), although it is still favourable in water solution.

Hydrogen bonds to the propionate side chain in haem

Finally, we studied how hydrogen bonds to the propionate side chains of the haem group are affected by metal binding in the centre of the porphyrin ring, using a water molecule as the probe. We compared a doubly protonated free porphyrin ring to haem groups with a Fe^{2+} or Fe^{3+} ion and coordinated by one axial imidazole ligand (as a models of the resting desoxy state of globins), both studied in the high-spin state. All side-chains of the porphyrin ring were included as can be seen in Figure 9.

From the results in Table 9, it can be seen that the hydrogen-bond strength is not much affected when a Fe^{2+} ion binds in the porphyrin ring. The water probe forms an O–HO hydrogen bond to each of the two carboxylate oxygen atom. In the free porphyrin, the two O–H distances are quite different, 1.76 and 2.23 Å, whereas in the Fe^{2+} complex, they are more similar, 1.85 and 2.02 Å. Nevertheless, the two complexes have almost the same hydrogen-bond energy, both in vacuum (79–80 kJ/mol) and in water solution (19 kJ/mol).

However, with Fe^{3+} in the ring, the two bonds become even more dissimilar than in the free porphyrin with O–H distances of 1.76 and 2.59 Å. Moreover, the hydrogen bonds become appreciably weaker: The hydrogen-bond strength goes down by over 22 kJ/mol to 57 kJ/mol. The reason for this is the reduced net charge of the complex: With free porphyrin and Fe^{2+}, the net charge is –2, but with Fe^{3+}, it is decreased to –1. This is confirmed by the decreased solvent effects, which ensure that in water solution, the Fe^{3+} complex actually has a slightly stronger hydrogen-bond energy by 4 kJ/mol.

All complexes give weaker hydrogen bonds than the free acetate–H_2O complex with the same type of double hydrogen bonds: It has two nearly symmetric hydrogen bonds with O–H distances of 1.93 and 1.97 Å, and a hydrogen-bond energy of 83 kJ/mol. However, the strength is reversed in water solution. This type of double hydrogen bond is stronger than the single anti bond found in the carboxypeptidase model and the corresponding free complex. However, in water solution, the free anti complex has a stronger hydrogen bond, 18 kJ/mol.

Discussion

We have investigated how metal coordination changes the hydrogen-bond properties of the ligands by studying over 60 complexes of nine different types. So far we have mainly discussed the hydrogen bonds within each type of complex and compared them to the corresponding free ligand. The test cases were designed to study how the hydrogen bonds are affected by at least five different properties, viz. the metal, the oxidation state, the ligand involved in the hydrogen bond, other first-sphere ligands, and different probe molecules. In this section, we will discuss the results of these comparisons over the various types of complexes.

Different metals

We have studied complexes with the six common first-row transition metals in biology, Mn, Fe, Co, Ni, Cu, and Zn. In three test cases (cytochrome, superoxide dismutase, and $MCys_4$) we compare different metals. These calculations quite clearly show that the strength of the hydrogen bonds is little affected by the type of metal, provided that the oxidation state (and therefore the net charge) is the same. The cytochrome models show differences in the NH–OH_2 distances of less than 0.05 Å between Fe, Co, and Ni, and differences of less than 3 kJ/mol in hydrogen-bond energies. Likewise, the superoxide-dismutase models show differences up to 0.03 Å for the NH–OH_2 distances and differences in the hydrogen-bond energies of up to 4 kJ/mol between Fe and Mn. For the $MCys_4$ models, the differences in the S–HOH distances are also up to 0.03 Å, but the difference in the hydrogen-bond energies is

12 kJ/mol between Fe and Zn. Thus, we can conclude that the nature of the metal has a minor effect on the hydrogen-bond strength, except for interactions involving Cys, which forms partly covalent Fe–S bonds, weakening hydrogen bonds to this ligand.

Different oxidation states

In five of the cases (cytochrome, peroxidase, superoxide dismutase, azurin, and porphyrin), we have studied how the oxidation state of the metal affects the hydrogen bonds. The results show that the oxidation state has a strong effect on the hydrogen-bond strength. For example, the hydrogen-bond energy increases by 14–17 kJ/mol when going from the +II to the +III oxidation state in the cytochrome models and the corresponding increase is 22–27 and 14–16 kJ/mol for the five- and six-coordinate superoxide dismutase models, respectively. However, the higher oxidation state does not always give the stronger hydrogen bond. For example, the hydrogen-bond strength to the porphyrin propionate group decreases when going from Fe^{2+} to Fe^{3+} by 24 kJ/mol, although the nearly identical hydrogen-bond energies with $2H^+$ or Fe^{2+} shows that the metal has little influence on this hydrogen bond (owing to the large distance). Instead, this decrease in hydrogen-bond energy simply reflects the decrease in the net charge of model from –2 to –1.

For the peroxidase Fe–OH models, the trends are even more complicated with hydrogen-bond energies of 84, 44, 26, and 35 kJ/mol for the formal Fe^{II}, Fe^{III}, Fe^{IV}, and Fe^{V} oxidation states and net charges of –1, 0, 1, and 2, respectively. In this case, the hydrogen-bond strength seems to be determined by a combination of the net charge and the electronic structure of the complexes. The first two complexes have the ion in the formal oxidation states with an OH^- ligand, and therefore, the hydrogen-bond strength reflects the decrease in the net charge of the complex. However, for the latter two complexes, the OH ligand acquires significant radical character and therefore also a lower charge, resulting in weaker hydrogen bonds. The difference between the Fe^{IV} and Fe^{V} complexes again reflects the net charge.

Finally, the azurin complexes show some interestingly trends when going from Cu^+ to Cu^{2+}: The two His ligands, show an expected 15-kJ/mol increase in the hydrogen-bond strength, owing to the increase in the net charge from 0 to +1. However, for the Met ligand, the Cu^+ complex actually gives a 1 kJ/mol stronger hydrogen bond, and for the Cys ligand, the hydrogen bond is 21 kJ/mol stronger for the reduced state, because the electron is removed both from Cys and from Cu. Therefore, we can conclude that the main effect on the oxidation state comes from the change in the net charge of the complex, the higher charge giving the stronger hydrogen bond. However, if the change in oxidation state affects also the ligand, this may alter the general trend. Again, sulphur-containing ligands give diverging trends.

Different ligands

For four of the test cases (the peroxidase, carboxypeptidase, azurin, and nitrite-reductase models), we have compared the hydrogen-bond strength of different ligands for the same type of complex. As discussed above for each test case, metal coordination almost always significantly affect the hydrogen-bond strength compared to the free ligand. Again, the net charge of the complex gives the largest effect. In general, the hydrogen-bond strength of neutral ligands is increased and that of the negatively charged ligands is decreased.

For the peroxidase models, we compared the hydrogen-bond strength of H_2O, OH^- and O^{2-}. When coordinated to Fe^{IV}, these ligands gave the opposite trend compared to the free ligands, with hydrogen-bond energies of 76, 44, and 34 kJ/mol, respectively. This is caused by the decreasing net charge of the three complexes, +2, +1, and 0. For the Fe^{IV}–OH^- model, we also compared states with OH^- as the donor and acceptor of the hydrogen bond. Again, the

result was opposite to that of the free ligand: The complex with an $^{-}OH–OH_2$ hydrogen bond (which does not exist in gas phase) was 18 kJ/mol stronger than the $^{-}HO–HOH$ state. We also compared the hydrogen-bond strength of the water and the imidazole ligands for the $Fe^{IV}–H_2O$ complex and showed that the former was 16 kJ/mol stronger, in variance to free complexes, for which the imidazole–OH_2 hydrogen bond is 5 kJ/mol stronger than the HOH–OH_2 hydrogen bond. Similar results were obtained for the nitrite-reductase models, for which we also compared H_2O and OH^- and again found the former to give the stronger hydrogen bond (76 compared to 40 kJ/mol), owing to the larger net charge of the water complex (+2 compared to +1). We also compared OH^- as a hydrogen-bond acceptor and donor, but this time it was 25 kJ/mol more favourable as an acceptor ($^{-}HO–HOH$).

For carboxypeptidase, we compared hydrogen bonds to Asp, His, and water ligands for the same complex (with a net charge of +1). It turned out that all three ligands gave quite similar energies, Asp being strongest (50 kJ/mol), and water weakest (46 kJ/mol). This again illustrates that the hydrogen bonds of charged ligands are strongly reduced, whereas those of neutral ligands are enhanced. In this case, water gives a weaker hydrogen bond than His, in contrast to what was found for the peroxidase models, showing that the relative strength depends on type of complexes.

Finally, we compared the five ligands of the azurin models, Cys, His (two different), Met, and a backbone carbonyl group. For the reduced state, we obtained the following trend for the hydrogen-bond strength: Cys > Met > His (no pure hydrogen bond to the back bond was obtained), whereas for the oxidised state, the trend was His > backbone > Met > Cys (the weak bond to Cys was discussed above). The most important conclusion from these trends is that the weak hydrogen bond to Met is more affected by the metal coordination than the stronger hydrogen bond to His, most likely reflecting the larger polarisability of the S atom.

Effect of the other ligands

For two model systems, we examined how variations in the other first- or second-sphere ligands affect the strength of hydrogen bonds to first-sphere metal ligands. For the protonated compound II models ($Fe^{IV}–OH^-$), we studied how the other axial ligand affected the HO–HOH hydrogen-bond strength. Again, we showed that the results depend primarily on the net charge of the complex (the hydrogen-bond strength was 30–38 kJ/mol for the neutral complexes and 26–30 kJ/mol for the complexes with a +1 net charge), but this time the complexes with the higher charge gave the lower hydrogen-bond strength. Moreover, models with His gave 4–8 kJ/mol lower hydrogen-bond energies than the other complexes with the same net charge.

For the superoxide-dismutase models, we compared five-coordinate models with either a bidentate Asp ligand or a monodentate Asp ligand and a water ligand. The result showed that the hydrogen-bond strengths changed by less than 4 kJ/mol for these models with the same net charge. However, if a superoxide ligand was added to the complex with both Asp and water, all hydrogen-bond strengths decreased by 16 kJ/mol for the M^{2+} models and by 24 kJ/mol for the M^{3+} models. Again, this reflects a decrease in the net charge of the complex by one unit.

We can also compare the hydrogen-bond strength of the same ligand in different types of complexes. For example, the imidazole–OH_2 interaction has been studied in five different types of complexes. In the cytochrome models, the hydrogen-bond strength was 24–27 kJ/mol for the neutral (M^{2+}) models and 39–41 kJ/mol for the +1 charged (M^{3+}) models. For the $Fe^{IV}(H_2O)$ peroxidase model, with a +2 net charge, it was even larger, 60 kJ/mol. In the superoxide dismutase models, it was 26–28 kJ/mol for the neutral models, 42–44 kJ/mol for the +1 models, and 65–70 kJ/mol for the +2 models. For the carboxypeptidase model (with a

+1 charge) it was 47 kJ/mol, and for the azurin it was 26–27 kJ/mol for the neutral reduced models and 40–41 kJ/mol for the oxidised (+1) models. Thus, we can conclude that the hydrogen-bond strength closely follows the net charge of the complex with variations of less than 10 kJ/mol between the different models that contain both different ligands and different metals.

The HOH–OH_2 interaction has been studied in three different complexes. In the $Fe^{IV}(H_2O)$ peroxidase model with its +2 net charge, the hydrogen-bond strength was 76 kJ/mol. In the carboxypeptidase model (with a +1 net charge) it was 47 kJ/mol, whereas in the nitrite-reductase model (with a +2 net charge) is was again 76 kJ/mol.

The $^{-}$OH–HOH hydrogen bond has been studied in three types of complexes. In the protonated compound II models, it had a hydrogen-bond strength of 26–30 kJ/mol for the complexes with a +1 net charge and 30–38 kJ/mol for the neutral complexes. For the peroxidase models, it is 84, 44, 26, and 35 kJ/mol for complexes with a net charge of –1, 0, 1, and 2, respectively, and for the nitrite-reductase models, it is 40 kJ/mol for a +1 model. In this case, it is clear that there is little correlation between the net charge of the complex and the hydrogen-bond strength, owing to the fact that the OH^- ligand often is partly oxidised in the complexes, which reduces its net charge and therefore its hydrogen-bond strength.

Finally, the CH_3S^-–HOH interaction has been studied in two types of complexes. In the $[Fe(SCH_3)_4]^{2-}$ model with a single hydrogen bond, the energy was 68 kJ/mol, whereas it was 46 and 25 kJ/mol in the azurin models with a net charge of 0 and +1. However, also for these models, the Cys ligand is partly oxidised.

Different probe molecules

Finally, we have used three different molecules to probe the hydrogen-bond strengths. In all test cases, we used water as the probe molecule, but for several peroxidase models, we tested also an imidazole group (as a model of the distal His residue) and in some nitrite-reductase models, we used also an acetate group as the probe (as a model of second-sphere Asp/Glu residues). Owing to the net charge of the latter group and also proton transfers, the latter results were varying.

However, the peroxidase models gave many interesting results. Like water, imidazole can both be a hydrogen-bond acceptor and donor. The results in Table 3 shows that imidazole always give appreciably stronger (65–19 kJ/mol) hydrogen bonds than water: With imidazole the strength of the hydrogen bonds to H_2O, OH^- (as donor), HO^- (as acceptor), and O^{2-} are 141, 85, 58, and 53 kJ/mol, respectively, compared to 76, 44, 26, and 34 kJ/mol for water. However, the order of the four complexes is the same with the two probe molecules, showing that the qualitative results are independent of the probe. The results are also in accordance with the isolated systems, for which imidazole also forms stronger hydrogen bonds to all three molecules.

Conclusions

In this paper we have studied how metal-coordination changes the hydrogen-bond strength of a ligand, based on state-of-the-art dispersion-corrected DFT calculations. We have studied over 60 complexes involving Mn, Fe, Co, Ni, Cu, Zn in various oxidation states and models of typical ligands found in biochemical systems, His, Asp, Glu, Cys, Met, as well as water molecules in three protonation states. To measure the hydrogen-bond strength, we have employed three types of probe molecules, water, imidazole (as a model of His), and acetate (as a model of Asp/Glu). The study has yielded much useful information.

In general, the hydrogen-bond strength is increased when neutral ligands coordinate to a

metal ion. The size of the increase depend on the net charge of the metal complex, as is shown in Figure 10a. For neutral complexes, the increase is modest, 0–17 kJ/mol in vacuum, which is reduced to up to 7 kJ/mol in water solution. For complexes with a +1 charge, the increase is 4–27 kJ/mol, which is reduced to less than 12 kJ/mol in water. For complexes with a double positive charge, the increase is much higher, 37–109 kJ/mol, but it is reduced to 1–37 kJ/mol in water. In only two cases, viz. for the hydrogen bonds to Met in the reduced and oxidised models of azurin, is the hydrogen-bond strength decreased and only in water solution (in both cases by 5 kJ/mol).

For negatively charged ligands, the hydrogen-bond strength is always decreased in vacuum by 2–143 kJ/mol. However, this is strongly modified by solvation effects and in water solution, the hydrogen-bond strength can increase by up to 19 kJ/mol (and even 144 kJ/mol for Fe^{IV}–O^{2-} complex) or decrease by up to 35 kJ/mol. From Figure 10b, it can be seen that again, the effect is mainly dictated by the net charge of the complex: For complexes with a net positive charge, the hydrogen-bond strength is decreased, whereas for negatively charged complexes, the hydrogen-bond strength is always increased, at least in water solution.

The importance of the net charge of the complex has been seen throughout this investigation. If the net charge does not change, there is little difference between different metals or other ligands. The only exception is when the ligand is involved in the redox chemistry, i.e. when there is significant spin density on the ligand. This happens primarily for Cys and OH^-.

Finally, metal-bonding often change trends observed for free ligands. For example, it strongly improves the hydrogen-bond donating ability of OH^- and inverts the relative hydrogen-bond strength of water and imidazole. Moreover, different types of complexes can show different trends: For example, in the peroxidase models, hydrogen bonds with OH^- as the donor were stronger than with it as the acceptor, whereas in the nitrite-reductase models, the opposite is observed. Thus, we have seen that metal-coordination has an important impact on hydrogen bonds of the ligand and such effects need to be considered in the understanding of metal sites in proteins or in the design of biomimetic inorganic models.

Acknowledgements

This investigation has been supported by grants from the Swedish research council (project 2010-5025) and by computer resources provided by the Swedish National Infrastructure for Computing (SNIC) at Lunarc at Lund University.

References

1 Jeffrey GA (1997) An introduction to hydrogen bonding, Oxford University Press, New York
2 Zhen Y-J, Merz KM (1992) J Comp Chem 13:1151-1169
3 Habermann SM, Murphy KP (1996) Prot Sci 5:1229-1239
4 Pudzianowski AT (1996) J Phys Chem 100:4781-4789
5 Gordon MS, Jensen JH (1996) Acc Chem Res 29:536-543
6 Tsuzuki S, Uchimaru T, Matsumura K, Mikami M, Tanabe K (1999) J Chem Phys 110:11906-11910
7 Halkier A, Klopper W, Helgaker T, Jorgensen P, Taylor PR (1999) J Chem Phys 111:9157-6167
8 Rappé AK, Bernstein ER (2000) J Phys Chem A 104:6117-6128

9 Scheiner S, Kar T, Pattanayak J (2002) J Am Chem Soc 13257-13264
10 Jurecka P, Sponer J, Cerny J, Hobza P (2006) Phys Chem Chem Phys 8:1985-1993
11 Riley KE, Hobza P (2007) J Phys Chem A 111:8257-8263
12 Riley KE, Pitonak M, Jurecka P, Hobza P (2010) Chem Rev 110:5023-5063
13 Rezac J, Riley KE, Hobza P (2011) J Chem Theory Comput 7:2427-2438
14 Goerigk L, Kruse H, Grimme S (2011) Chem Phys Chem 12:3421-3433
15 Thanthiriwatte KS, Hohenstein EG, Burns LA, Sherrill CD (2011) J Chem Theory Comput 7:88-96
16 C. F. Baes, R. E. Mesmer, The hydrolysis of cations. Wiley, New York, 1976.
17 Holm RH, Kennepohl P, Solomon EI (1996) Chem Rev 96:2239-2314
18 N. Källrot, K. Nilsson, T. Rasmussen, Ryde U (2005) "The structure of the catalytic copper site in nitrite reductase, studied by quantum refinement", Intern. J. Quant. Chem., 102, 520-541
19 Ryde U (1996) "The coordination chemistry of the structural zinc ion in alcohol dehydrogenase studied by ab initio quantum chemical calculations". Eur. Biophys. J. 24, 213-221
20 Poulos TL (1987) Adv Inorg Biochem 7:1–36
21 Kaim W, Schwederski B (1994) Bioinorganic Cemistry: Inorganic elements in the chemistry of life, John Wiley & Sons, Chichester
22 P. Rydberg, E. Sigfridsson, Ryde U (2004) "On the role of the axial ligand in haem proteins - a theoretical study", J. Biol. Inorg. Chem., 9, 203-223
23 Epstein LM, Shubina ES (2002) Coord Chem Rev 231:165-181
24 Falvello LR (2010) Angew Chem Int Ed 49:10045-10047
25 Helm L, Merbach AE (1999) Coord Chem Rev 187:151-181
26 Kropman MF, Bakker HJ (2001) Science 291:2118-2120
27 R. Mancinell, A. Botti, F. Bruni, M. A. Ricci and A. K. Soper, Phys. Chem. Chem. Phys., 2007, 9, 2959
28 D. Paschek and R. Ludwig, Angew. Chem., Int. Ed., 2011, 50, 352
29 Bustamante M, Vlencia I, Castro M (2011) J Phys Chem A 115:4115-4134
30 Prell JS, O'Brien JT, Williams ER (2011) J Am Chem Soc 133:4810-4818
31 Pavlov M, Siegbahn PEM, Sandström M (1998) J Phys Chem A 102:219-228
32 Rode BM, Schwenk CF, Hofer TS, Randolf BR (2005) Coord Chem Rev 249:2993-
33 Ryde U (1994) "The coordination chemistry of the catalytic zinc ion in alcohol dehydrogenase studied by ab initio quantum chemical calculations". Int. J. Quant. Chem. 52, 1229-1243
34 Andric JM, Janjic GV, Ninkovic DB, Zaric SD (2012) Phys Chem Chem Phys 14:10896-10898
35 Schmiedekamp A, Nanda V (2009) J Inorg Biochem 103:1054-1060
36 Wirstam M, Lippard SJ, Friesner RA (2003) J Am Chem Soc 125:3980-3987
37 E. Sigfridsson, U. Ryde (1999) "On the significance of hydrogen bonds for the discrimination between CO and O_2 by myoglobin". J. Biol. Inorg. Chem., 4, 99-110.
38 Ryde U, M. H. M. Olsson, B. O. Roos, K. Pierloot, J. O. A. De Kerpel (2000) "On the role of strain in blue copper proteins". J. Biol. Inorg. Chem., 5, 565-574
39 Ryde U (1999) "Carboxylate binding modes in zinc proteins, a theoretical study". Biophys. J. 77, 2777-2787.
40 K. P. Jensen, Ryde U (2003) "Importance of proximal hydrogen bonds in haem proteins", Mol. Phys., 101, 2003-2018.
41 K. Nilsson, H.-P. Hersleth, T. H. Rod, K. K. Andersson, Ryde U (2004) "The protonation status of compound II in myoglobin, studied by a combination of

experimental data and quantum chemical calculations: quantum refinement", Biophys. J., 87, 3437-344
42 J. Heimdal, P. Rydberg, Ryde U (2008) " Protonation of the proximal histidine ligand in haem peroxidases", J. Phys. Chem. B., 112, 2501-2510.
43 E. Sigfridsson, M. H. M. Olsson, Ryde U (2001) "Inner-sphere reorganization energy of iron–sulphur clusters studied by theoretical methods", Inorg. Chem., 40, 2509-2519
44 E. Sigfridsson, M. H. M. Olsson, Ryde U (2001) "A comparison of the inner-sphere reorganisation energies of cytochromes, iron-sulphur clusters, and blue copper proteins", J. Phys. Chem. B, 105, 5546-5552.
45 K. P. Jensen, Ryde U (2003) "Comparison of the chemical properties of iron and cobalt porphyrins and corrins", ChemBioChem, 4, 413-424
46 K. P. Jensen, Ryde U (2005) "Comparison of chemical properties of iron, cobalt, and nickel porphyrins, corrins, and hydrocorphins", J. Porph. Phthalocyanines, 9, 581-606.
47 L. Rulíšek, K. P. Jensen, K. Lundgren, Ryde U (2006) "The reaction mechanism of iron and manganese superoxide dismutases studied by theoretical methods", J. Comput. Chem., 27, 1398-1414
48 A. D. Becke, *Phys. Rev. A* **1988**, *38*, 3098-3100.
49 J. P. Perdew *Phys. Rev. B* **1986**, *33*, 8822-8824
50 A. Schäfer, H. Horn, and R. Alrichs, *J. Chem. Phys*. **1992**, *97*, 2571.
51 A. Schäfer, C. Huber, R. Ahlrichs, *J. Chem. Phys*. **1994**, *100*, 5829.
52 W. J Hehre, L. Radom, P. v. R. Schleyer, J. A. Pople Ab initio molecular orbital theory, Wiley-Interscience, New York, **1986**.
53 K. Eichkorn, O. Treutler, H. Öhm, M. Häser, R. Ahlrichs, *Chem. Phys. Lett.* **1995**, *240*, 283-290.
54 K. Eichkorn, F. Weigend, O. Treutler, R. Ahlrichs, *Theor Chem Acc*. **1997**, *97*, 119-126
55 Lee, C., Yang, W., Parr, R.G., Phys. Rev. B 37 (1988), 785.
56 Becke, A.D., J. Chem. Phys. 98 (1993), 5648
57 Klamt, A.; Schüürmann, J. *J Chem Soc Perkin Trans 2* **1993,** *5*, 799-805.
58 Schäfer, A.; Klamt A.; Sattel, D.; Lohrenz, J. C. W.; Eckert, F. Phys. Chem. Chem. Phys. 2000, 2, 2187-2193.
59 Klamt, A.; Jonas, V.; Bürger, T.; Lohrenz, J. C. W. *J. Phys. Chem.,* **1998,** *102,* 5074-5085.
60 Sharp, K. A. Annu Rev Biophys Biophys Chem 1990, 19, 301.
61 Honig, B. Science 1995, 268, 1144.
62 Treutler, O.; Ahlrichs, R. *J. Chem. Phys.* **1995**, *102*, 346-354.
63 S. Grimme, J. Antony, S. Ehrlich, H. Krieg, J. Chem. Phys. 2010, 132, 154104.
64 http://toc.uni-muenster.de/DFTD3/getd3.html
65 Miertus, S; Scrocco, E.; Tomasi, J. Chem. Phys. 1981, 55, 117.
66 Tomasi, J.; Mennucci, B.; Cammi, R. Chem. Rev. 2005, 105, 2999-3093.
67 Gaussian 03, Revision D.01, Frisch, M. J.; Trucks, G. W.; Schlegel, H. B.; Scuseria, G. E.; Robb, M. A.; Cheeseman, J. R.; Montgomery, Jr., J. A.; Vreven, T.; Kudin, K. N.; Burant, J. C.; Millam, J. M.; Iyengar, S. S.; Tomasi, J.; Barone, V.; Mennucci, B.; Cossi, M.; Scalmani, G.; Rega, N.; Petersson, G. A.; Nakatsuji, H.; Hada, M.; Ehara, M.; Toyota, K.; Fukuda, R.; Hasegawa, J.; Ishida, M.; Nakajima, T.; Honda, Y.; Kitao, O.; Nakai, H.; Klene, M.; Li, X.; Knox, J. E.; Hratchian, H. P.; Cross, J. B.; Bakken, V.; Adamo, C.; Jaramillo, J.; Gomperts, R.; Stratmann, R. E.; Yazyev, O.; Austin, A. J.; Cammi, R.; Pomelli, C.; Ochterski, J. W.; Ayala, P. Y.; Morokuma, K.; Voth, G. A.; Salvador, P.; Dannenberg, J. J.; Zakrzewski, V. G.; Dapprich, S.; Daniels, A. D.; Strain, M. C.; Farkas, O.; Malick, D. K.; Rabuck, A. D.; Raghavachari, K.; Foresman, J. B.; Ortiz, J. V.; Cui, Q.; Baboul, A. G.; Clifford, S.; Cioslowski, J.; Stefanov, B. B.; Liu, G.;

Liashenko, A.; Piskorz, P.; Komaromi, I.; Martin, R. L.; Fox, D. J.; Keith, T.; Al-Laham, M. A.; Peng, C. Y.; Nanayakkara, A.; Challacombe, M.; Gill, P. M. W.; Johnson, B.; Chen, W.; Wong, M. W.; Gonzalez, C.; and Pople, J. A.; Gaussian, Inc., Wallingford CT,
68 Ryde U, R. A. Mata, S. Grimme "Does DFT-D estimate accurate energies for the binding of ligands to metal complexes?" Dalton Trans., 2011, 111, 3949-3960.
69 Boys SF, Bernardi F (1970) Mol Phys 19:553-566
70 Green MT (2009) Curr Opin Chem Biol 13:84-88
71 Shaik S, Cohen S, Wang Y, Chen H, Kumar D, Thiel W (2010) Chem Rev 110:949-1017
72 Shepard WEB, Anderson BF, Lewandoski DA, Norris GE, Bake EN (1990) J Am Chem Soc 112:7817-7819
73 Baker EN (1988) J Mol Biol 203:1071-1095

Table 1. Results for the protonated compound II models (Fe^{IV}Por(OH)Ax) with different axial ligands (Ax). The table shows the net charge (Ch) and number of unpaired spins (Spin) on the various complexes, as well as the average Fe–N distances to the four N atoms in the porphine ring (N_{av}), the Fe–O distance to OH^-, the Fe distance to the axial ligand, the O–H distance of the HO–HOH hydrogen bond (i.e. the distance between the O atom of the OH^- ligand and one of the H atoms of the water probe; all distances are in Å), the Mulliken spin densities on the Fe ion, the porphyrin ring (Por), the OH group, and the axial ligand (the spin on the second-sphere ligand and the water probe was always <0.01 *e*). Finally, the energy of the HO–HOH hydrogen bond is given in kJ/mol for three values of the dielectric constant (1, 4, and 80) in the COSMO continuum-solvation calculations.

Axial	Probe	Ch	Spin	Distance to Fe				Spin on				Energy		
ligand				N_{av}	O	Ax	O–H	Fe	Por	OH	Ax	1	4	80
Cys	H_2O	0	2	2.02	1.86	2.26	1.81	1.81	-0.21	0.13	0.24	38.1	28.1	21.6
	no	0	2	2.02	1.84	2.27		1.82	-0.23	0.17	0.21			
His	H_2O	1	2	2.01	1.81	2.01	1.85	1.87	-0.02	0.12	-0.01	25.7	14.0	3.2
	no	1	2	2.01	1.79	2.05		1.92	-0.09	0.17	-0.02			
His+Asp	H_2O	0	2	2.01	1.84	1.95	1.80	1.88	-0.18	0.13	0.14	30.4	20.4	14.3
	no	0	2	1.99	1.82	2.02		1.91	-0.24	0.17	0.10			
Tyr	H_2O	0	2	2.01	1.83	1.85	1.79	1.62	-0.20	0.08	0.51	35.2	24.1	16.9
	no	0	2	2.01	1.82	1.86		1.66	-0.21	0.11	0.45			
Tyr+Arg	H_2O	1	2	2.01	1.82	1.94	1.83	2.08	-0.27	0.11	0.03	29.6	19.8	13.8
	no	1	2	2.01	1.80	1.95		2.05	-0.27	0.15	0.03			
HO^-+HOH		-1	0				1.23					117.4	59.6	30.8

Table 2. Results for the cytochrome models ($MPorIm_2$) with different metals. The entries are the same as in Table 1 and the spin on the water probe was always <0.01 *e*.

Metal	Probe	Ch	Spin	Distance to Fe				Spin on				Energy		
				N_{av}	N_{Im1}	N_{Im2}	O–H	Fe	Por	Im_1	Im_2	1	4	80
Fe^{2+}	H_2O	0	0	2.01	1.99	1.99	1.90					26.8	15.4	8.6
	no	0	0	2.01	1.99	1.99								
Co^{2+}	H_2O	0	1	2.00	2.28	2.25	1.95	1.20	-0.26	0.03	0.05	23.7	13.6	7.6
	no	0	1	2.00	2.26	2.27		1.23	-0.29	0.04	0.04			
Ni^{2+}	H_2O	0	2	2.06	2.15	2.16	1.94	2.61	-0.43	-0.07	-0.09	24.9	14.3	8.0
	no	0	2	2.06	2.15	2.16		2.62	-0.43	-0.08	-0.08			
Fe^{3+}	H_2O	1	1	2.01	1.99	2.00	1.85	0.95	0.06	0.00	0.00	41.4	19.7	7.7
	no	1	1	2.01	1.99	1.99		0.75	0.12	0.03	0.03			
Co^{3+}	H_2O	1	0	2.01	1.96	1.95	1.84					41.0	20.4	9.1
	no	1	0	2.01	1.95	1.95								
Ni^{3+}	H_2O	1	1	2.01	2.14	2.17	1.86	1.59	-0.59	0.03	0.00	38.7	19.0	8.3
	no	1	1	2.01	2.16	2.16		1.66	-0.63	0.00	0.00			
$Im+OH_2$		0	0				1.97					23.4	13.8	7.8

Table 3. Results for the peroxidase models (FePorImAx) with Fe in different oxidation states (Ox), with either H_2O, OH^-, or O^{2-} as the second axial ligand (Ax), and either water, imidazole (either acceptor, HID, or donor, HIE), or imidazolium (HIP) as the hydrogen-bonding probe. The entries are the same as in Table 1.

Ox	Ax	Probe	Ch	Spin	Distance to Fe				Spin on					Energy		
					N_{av}	N_{Im}	O	O–H	Fe	Por	Im	Ax	Probe	1	4	80
II	OH	HOH	-1	0	2.01	1.94	2.02	1.63						84.3	63.4	49.7
		no	-1	0	2.01	1.91	2.04									
III	OH	HOH	0	1	2.02	1.84	2.04	1.76	1.12	-0.14	-0.02	-0.01	0.00	43.8	32.6	24.8
		no	0	1	2.02	1.82	2.06		0.97	-0.14	-0.01	0.12	0.00			
IV	OH	HOH	1	2	2.01	1.81	2.01	1.85	1.87	-0.02	-0.01	0.12	0.00	25.7	14.0	3.2
		no	1	2	2.01	1.79	2.05		1.92	-0.09	-0.02	0.17	0.00			
V	OH	HOH	2	1	2.00	1.81	2.03	1.94	1.00	-0.07	-0.02	0.12	-0.01	34.8	13.1	2.0
		no	2	1	2.00	1.79	2.04		1.95	-1.14	-0.02	0.19	0.00			
IV	H_2O	OH_2[a]	2	2	1.98	2.05	1.93	1.73	1.01	0.99	-0.02	0.00	0.00	60.2	26.5	8.8
		no	2	2	1.98	2.04	1.94		1.00	0.99	-0.01	0.00	0.00			
IV	H_2O	OH_2	2	2	1.98	2.00	1.98	1.60	0.98	1.00	-0.01	0.00	0.00	76.5	44.8	27.9
		no	2	2	1.97	2.05	1.98		0.99	1.03	-0.02	0.00	0.00			
IV	OH	OH_2	1	2	2.02	1.76	2.02	1.71	1.91	-0.16	-0.02	0.25	0.00	43.7	26.4	17.8
		no	1	2	2.01	1.79	2.02		1.92	-0.10	-0.01	0.17	0.00			
IV	O	HOH	0	2	2.06	1.66	2.02	1.82	1.43	-0.21	-0.02	0.78	0.00	34.0	23.9	16.4
		no	0	2	2.06	1.65	2.02		1.37	-0.22	-0.03	0.87	0.00			
IV	H_2O	HID	2	2	1.98	1.96	1.96	1.59	0.97	1.00	0.00	0.02	0.00	141.5	86.7	57.2
		no	2	2	1.98	2.05	1.94		0.96	1.03	-0.01	0.00	0.00			
IV	OH	HID	1	2	2.04	1.71	2.01	1.39	1.79	-0.22	0.01	0.41	-0.02	85.4	59.2	44.3
		no	1	2	2.01	1.79	2.02		1.92	-0.10	-0.01	0.17	0.00			
IV	OH	HIE	1	2	2.01	1.83	2.00	1.75	0.98	0.61	0.34	0.10	0.00	57.7	38.4	28.5
		no	1	2	2.01	1.79	2.05		1.92	-0.08	-0.02	0.17	0.00			
IV	OH	HIP	2	2	2.01	1.87	1.95	1.52	1.00	0.90	0.00	0.07	0.00	-54.6	7.5	34.5
		no	1	2	2.00	1.79	2.05		1.92	-0.10	-0.02	0.17	0.00			
IV	O	HIE	0	2	2.06	1.66	2.02	1.80	1.48	-0.24	-0.02	0.76	0.00	52.5	36.9	24.4
		no	0	2	2.06	1.65	2.02		1.37	-0.22	-0.03	0.87	0.00			
IV	O	HIP	1	2	2.05	1.69	2.02	1.26	1.70	-0.21	0.01	0.51	-0.02	186.6	82.3	27.7
		no	0	2	2.06	1.65	2.02		1.37	-0.22	-0.03	0.87	0.00			
$HOH+OH_2$			0	0				1.91						18.9	12.1	8.4
HO^-+HOH			-1	0				1.23						117.4	59.6	30.8
$O^{2-}+HOH$			-2	0				1.51						176.8	58.1	3.8
$Im+OH_2$			0	0				1.97						23.4	13.8	7.8
Im+HOH			0	0				1.87						32.2	24.7	19.8
$Im+OH^-$			-1	0				1.48						170.7	83.3	40.0
$Im+O^{2-}$			-2	0				1.34						188.6	-23.6	-119.5
ImH^++OH^-			0	0				1.26						584.4	229.5	65.1
ImH^++O^{2-}			-1	0				1.07						1103.1	311.0	-51.0

[a] The probe binds to the imidazole ligand, rather than to water.

Table 4. Results for the superoxide-dismutase models with Fe and Mn in the +2 and +3 oxidation states and four (MIm_3Ac), five (also H_2O), or six (also O_2^-) ligands. The entries are the same as in Table 1. The spin on the water ligand and the water probe were always <0.01 *e*.

Metal	Probe	Ch	Spin	Distance to Fe					Spin on				Energy		
				N_{av}	O_{Ac1}	O_{Ac2}		N–H	M	Im_{av}	Ac	O_2	1	4	80
Four-coordinate models									3.89	0.00	0.10		41.8	20.4	9.1
Fe^{2+}	H_2O	1	4	2.08	2.04	2.30		1.84	3.88	0.00	0.11				
	no	1	4	2.09	2.04	2.29			4.97	-0.02	0.07		42.5	21.1	9.7
Mn^{2+}	H_2O	1	5	2.16	2.13	2.28		1.83	4.83	0.02	0.09				
	no	1	5	2.16	2.13	2.27			4.35	0.10	0.33		65.2	28.2	9.3
Fe^{3+}	H_2O	2	5	2.04	2.06	2.10		1.70	4.34	0.09	0.34				
	no	2	5	2.04	2.06	2.09			4.10	-0.04	0.01		69.7	31.9	12.6
Mn^{3+}	H_2O	2	4	2.02	1.94	2.10		1.67	4.09	-0.04	0.00				
	no	2	4	2.02	1.93	2.10									
Five-coordinate models				N_{av}	O_{Ac}	O_{Wat}									
Fe^{2+}	H_2O	1	4	2.12	1.98	2.22		1.82	3.89	0.01	0.08		42.2	19.9	8.0
	no	1	4	2.13	1.98	2.21			3.88	0.01	0.08				
Mn^{2+}	H_2O	1	5	2.20	2.05	2.23		1.82	4.97	-0.01	0.02		44.2	21.6	9.4
	no	1	5	2.20	2.05	2.22			4.97	-0.01	0.02				
Fe^{3+}	H_2O	2	5	2.08	1.90	2.11		1.69	4.36	0.09	0.32		66.0	28.6	9.4
	no	2	5	2.08	1.90	2.09			4.36	0.09	0.33				
Mn^{3+}	H_2O	2	4	2.04	2.07	1.86		1.69	4.11	-0.05	0.02		66.1	28.8	9.6
	no	2	4	2.05	2.08	1.85			4.11	-0.05	0.02				
Six-coordinate models				N_{av}	O_{Ac}	O_{Wat}	O_{O2}								
Fe^{2+}	H_2O	0	5	2.21	2.19	2.21	1.86	1.94	3.84	0.02	0.05	1.00	25.9	14.5	7.0
	no	0	5	2.22	2.19	2.20	1.86		3.83	0.03	0.05	1.00			
Mn^{2+}	H_2O	0	6	2.27	2.22	2.31	2.17	1.91	4.94	-0.01	0.01	1.05	28.1	17.3	10.6
	no	0	6	2.27	2.30	2.30	2.17		4.93	0.00	0.01	1.04			
Fe^{3+}	H_2O	1	6	2.16	2.05	2.12	2.17	1.84	4.10	0.03	0.10	1.65	42.3	21.5	10.0
	no	1	6	2.16	2.04	2.11	2.16		4.09	0.04	0.10	1.65			
Mn^{3+}	H_2O	1	3	2.19	1.98	2.23	1.91	1.84	4.37	-0.02	-0.01	-1.36	41.9	20.5	8.8
	no	1	3	2.19	1.98	2.23	1.91		4.37	-0.02	-0.01	-1.36			
$Im+OH_2$		0	0					1.97				1.97	19.2	9.6	3.5

Table 5. Results for the $MCys_4$ models with either Fe^{2+} or Zn^{2+} and water binding either to one or two of the ligands. The entries are the same as in Table 1. The spin on the water probe was always <0.01 *e*.

Metal	Probe	Ch	Spin	Distances (Å)			Spin on		Energy		
				$Fe–S_{av}$	$S_1–H_1$	$S_2–H_2$	Fe	Cys_{av}	1	4	80
Fe^{2+}	H_2O	-2	4	2.36	2.19		3.53	0.11	67.5	29.5	9.5
	H_2O	-2	4	2.36	2.35	2.44	3.55	0.10	71.9	37.8	19.3
	no	-2	4	2.36			3.52	0.12			
Zn^{2+}	H_2O	-2	0	2.42	2.32	2.41			84.0	44.7	23.8
	no	-2	0	2.42							
CH_3S^-+HOH		-1	0		2.15				66.1	33.2	15.4

Table 6. Results for the carboxypeptidase models ($[ZnIm_2Ac(H_2O)]^+$) with the water probe molecule binding to different ligands. The entries are the same as in Table 1. The spin on the water probe was always <0.01 *e*.

Acceptor	Probe			Distance to Fe				Energy		
		Ch	Spin	N_{av}	N_{Im1}	N_{Im2}	O–H	1	4	80
	no	1	0	2.01	1.96	2.02				
water	H_2O	1	0	2.02	1.96	2.01	1.74	45.8	29.4	20.6
imidazole	H_2O	1	0	2.01	1.96	2.02	1.80	46.9	23.4	10.8
acetate	H_2O	1	0	2.00	1.98	2.03	1.81	50.4	25.7	12.6
$HOH+OH_2$		0	0				1.91	18.9	12.1	8.4
$Im+OH_2$		0	0				1.97	23.4	13.8	7.8
Ac^-+HOH	anti	-1	0				1.57	70.2	34.8	17.7

Table 7. Results for the azurin models ($Cu(SCH_3)$(imidazole)(imidazole–$CH_2CH_2NHCOCH_3$)(CH_3SCH_3)) in the Cu^+ and Cu^{2+} states with the water probe binding to different ligands (BB = backbone). The entries are the same as in Table 1. The distances to the Met ligand and the backbone carbonyl group were fixed to distances found in crystal structures of reduced (3.21 and 3.25 Å) and oxidised azurin (3.16 and 3.12 Å) [72,73]. The spin on the water probe and the Met ligand was always <0.01 *e*.

Acceptor	Probe	Ch	Spin	Distance (Å)			Spin on				Energy		
				$Cu–N_{av}$	$Cu–S_{Cys}$	O–H	Cu	Cys	His_1	His-BB	1	4	80
Cu^+ models													
	no	0	0	2.03	2.20								
His1	H_2O	0	0	2.03	2.20	1.94					25.8	15.7	9.6
His2	H_2O	0	0	2.03	2.20	1.93					26.6	15.7	9.0
Cys	H_2O	0	0	2.02	2.21	2.14					45.6	32.5	25.1
Met	H_2O	0	0	2.05	2.19	2.23					34.9	15.5	4.6
BB+Cys	H_2O	0	0	2.04	2.19	2.02					54.1	46.6	42.1
Cu^{2+} models													
	no	1	1	2.00	2.16		0.32	0.58	0.05	0.05			
His1	H_2O	1	1	2.00	2.16	1.85	0.33	0.57	0.05	0.05	39.9	20.0	9.2
His2	H_2O	1	1	2.00	2.16	1.85	0.33	0.57	0.05	0.05	41.2	20.6	9.1
Cys	H_2O	1	1	2.00	2.18	2.44	0.39	0.48	0.09	0.02	24.6	7.9	-1.3
Met	H_2O	1	1	2.00	2.16	2.37	0.33	0.56	0.05	0.05	33.6	14.8	4.3
BB	H_2O	1	1	2.01	2.16	1.74	0.32	0.57	0.05	0.02	38.8	24.0	15.9
$Im+OH_2$		0	0			1.97					23.4	13.8	7.8
CH_3S^-+HOH		-1	0			2.15					66.1	33.2	15.4
$(CH_3)_2S$+HOH		0	0			2.43					17.6	12.4	9.5
$CH_3CONHCH_3$+HOH		0	0			1.80					34.4	23.2	16.3

Table 8. Results for the nitrite-reductase models ($Cu^{2+}Im_3X$) with X = H_2O or OH^-, and different probe molecules (H_2O, Ac, or HAc) binding to the X ligand. The entries are the same as in Table 1. The spin on the probe molecule was always <0.01 *e*.

X	Probe	Ch	Spin	Distance (Å)			Spin on			Energy		
				$Cu–N_{av}$	Cu–O	O–H	Cu	Im_{av}	X	1	4	80
H_2O	no	2	1	1.97	2.18		0.66	0.10	0.02			
OH	no	1	1	2.03	1.89		0.58	0.06	0.23			
H_2O	OH_2	2	1	1.98	2.07	1.60	0.65	0.10	0.04	75.9	29.8	11.9
OH	OH_2	1	1	2.03	1.89	1.80	0.56	0.05	0.29	15.3	-13.8	-21.8
OH	HOH	1	1	2.02	1.91	1.70	0.59	0.07	0.18	39.8	14.0	7.6
OH	HAc	1	1	2.02	1.91	1.57	0.62	0.06	0.19	68.8	35.9	29.5
H_2O	Ac	1	1	1.99	2.36	1.62	0.60	0.05	0.23	666.6	157.1	-64.5
HOH+OH_2		0	0			1.91				18.9	12.1	8.4
HO^-+HOH		-1	0			1.23				117.4	59.6	30.8
HAc+OH^-		-1	0			1.36				170.7	98.5	64.9
Ac^-+HOH		-1	0			1.57				70.2	34.8	17.7
Im+Ac^-		-1	0			1.54				120.7	56.2	22.8

Table 9. Results for the porphyrin ring with all side chains and different metal ions in the centre (or two protons). The entries are the same as in Table 1. The spin on the water probe was always <0.01 *e*.

Metal	Probe			Distance (Å)				Spin on			Energy		
		Ch	Spin	Fe–N_{av}	Fe–N_{Im}	O_1–H_1	O_2–H_2	Fe	Por	Im	1	4	80
H_2	HOH	-2	0			1.76	2.23				78.8	41.8	19.4
	no	-2	0										
Fe^{2+}	HOH	-2	4	2.08	2.16	1.85	2.02	3.92	0.07	0.00	80.3	41.8	19.1
	no	-2	4	2.08	2.16			3.92	0.05	0.00			
Fe^{3+}	HOH	-1	5	2.08	2.14	1.76	2.59	4.10	0.83	0.04	56.7	40.7	23.3
	no	-1	5	2.08	2.14			4.06	0.88	0.03			
Ac^-+HOH		-1	0			1.93	1.97				82.6	38.3	14.5

Figure 1. The five protonated compound II models with different axial ligands, His (a), His+Asp (b), Cys (c), Tyr (d), and Tyr+Arg (e).

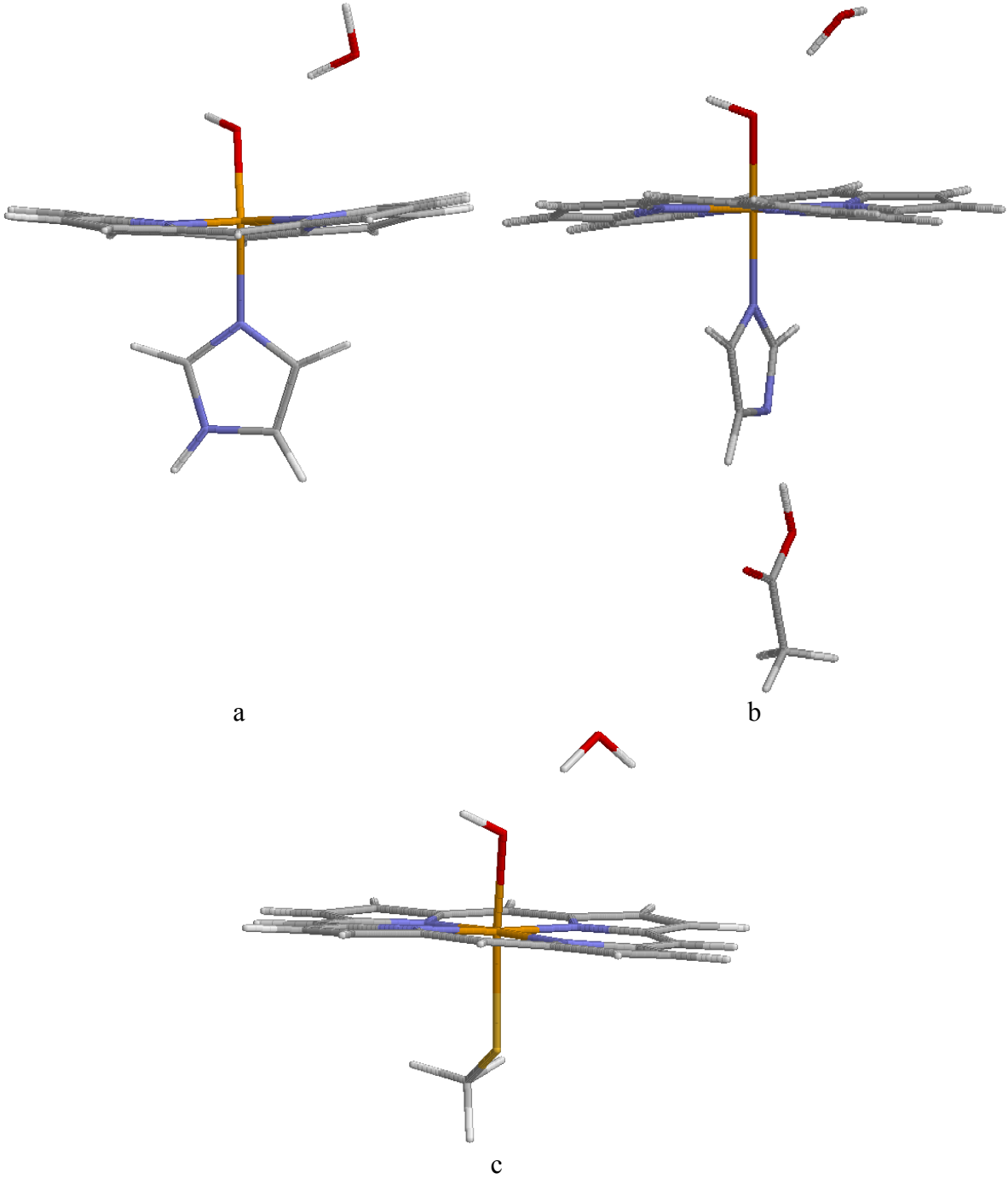

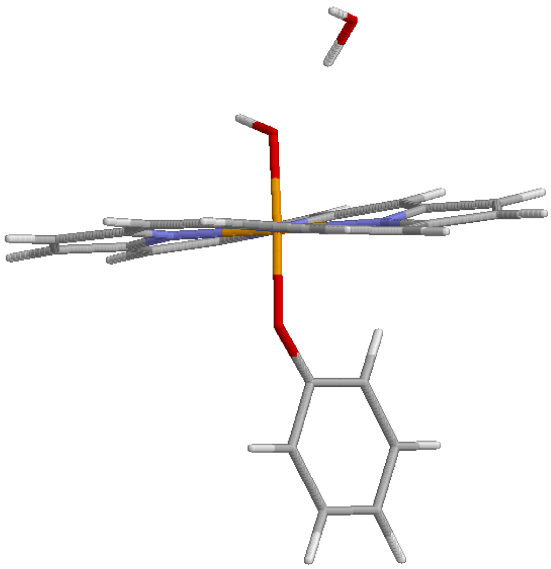

d

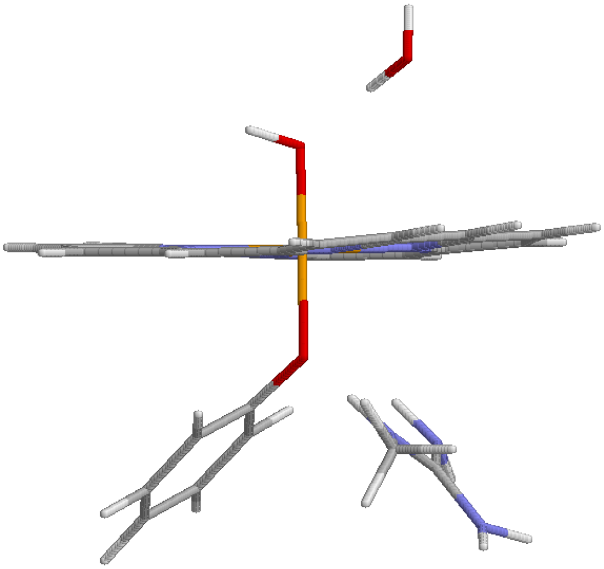

e

Figure 2. The cytochrome model, using the Fe^{2+} complex as an example.

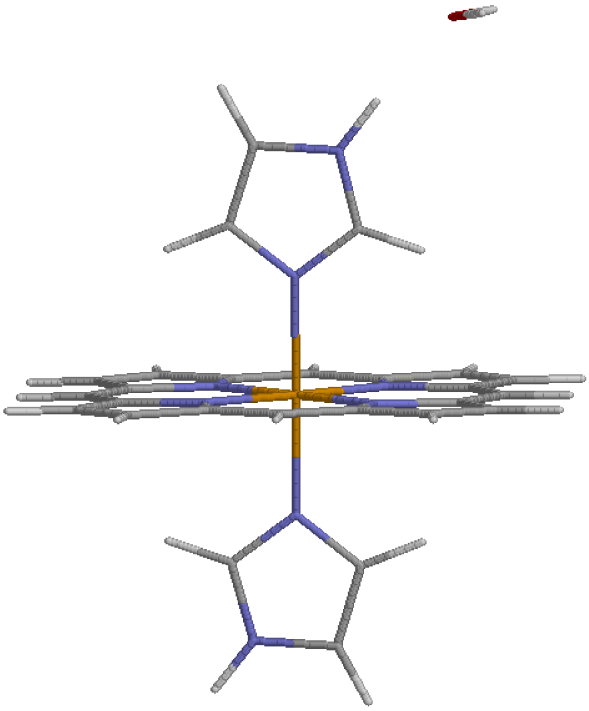

Figure 3. Eleven different types of peroxidase models studied: Fe^{IV}–H_2O with water hydrogen bonded to either imidazole (a) or the water ligand (b), Fe^{IV}–OH^- both as the donor (c) and acceptor (d), Fe^{IV}–O^{2-} (e), Fe^{IV}–H_2O+HID (f), Fe^{IV}–OH^-+HID (g), Fe^{IV}–OH^-+HIE (h), Fe^{IV}–OH^-+HIP (i), Fe^{IV}–O^{2-}+HIE(j), and Fe^{IV}–O^2+HIP (k).

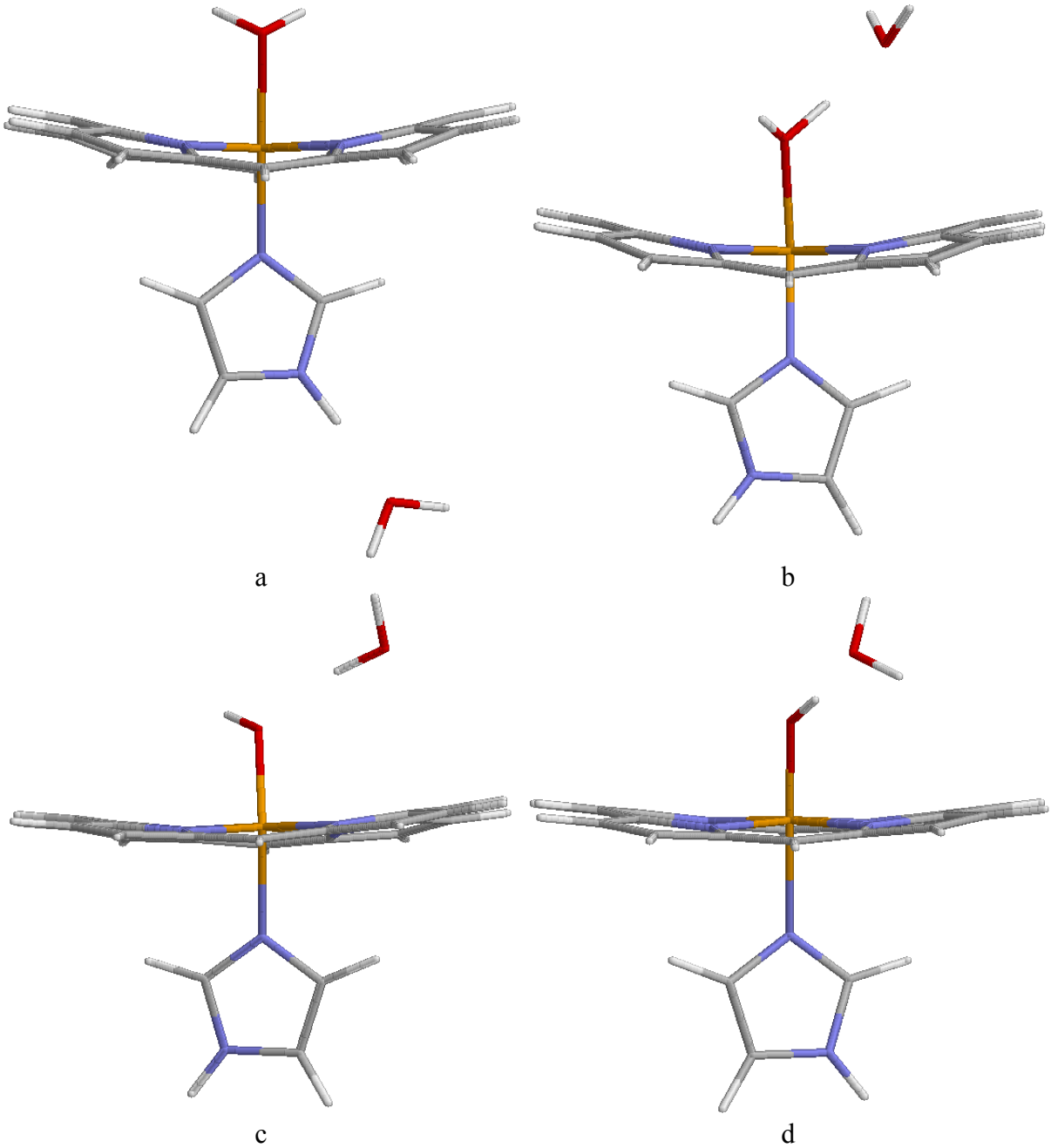

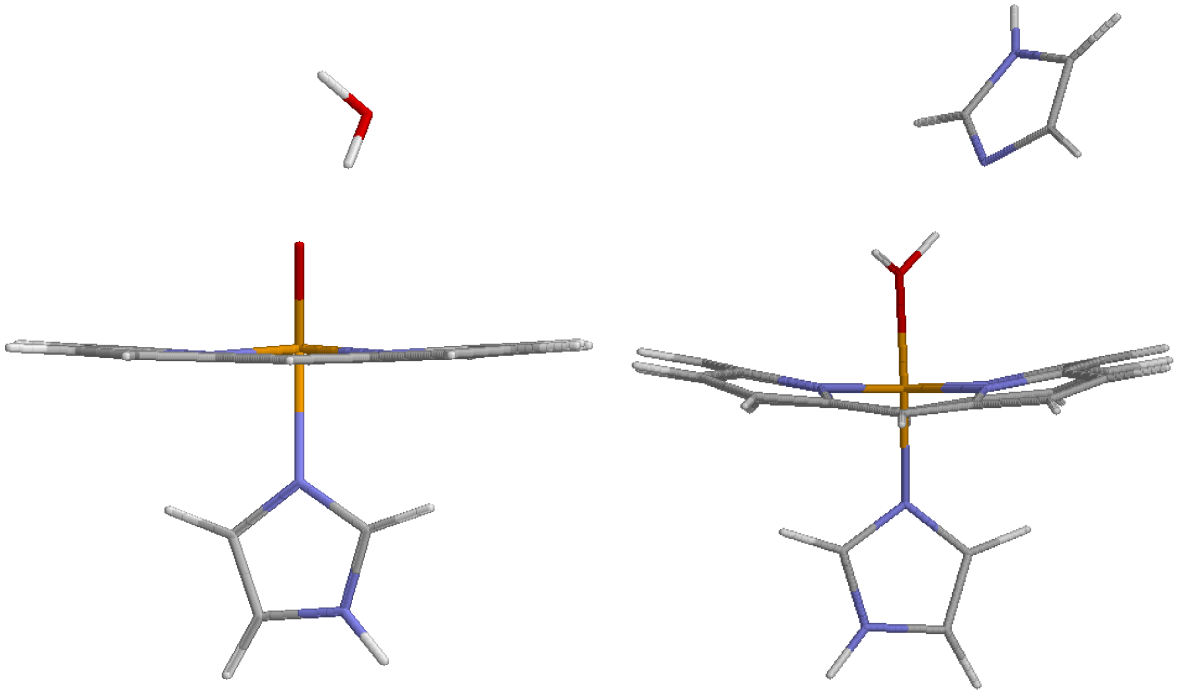

e f

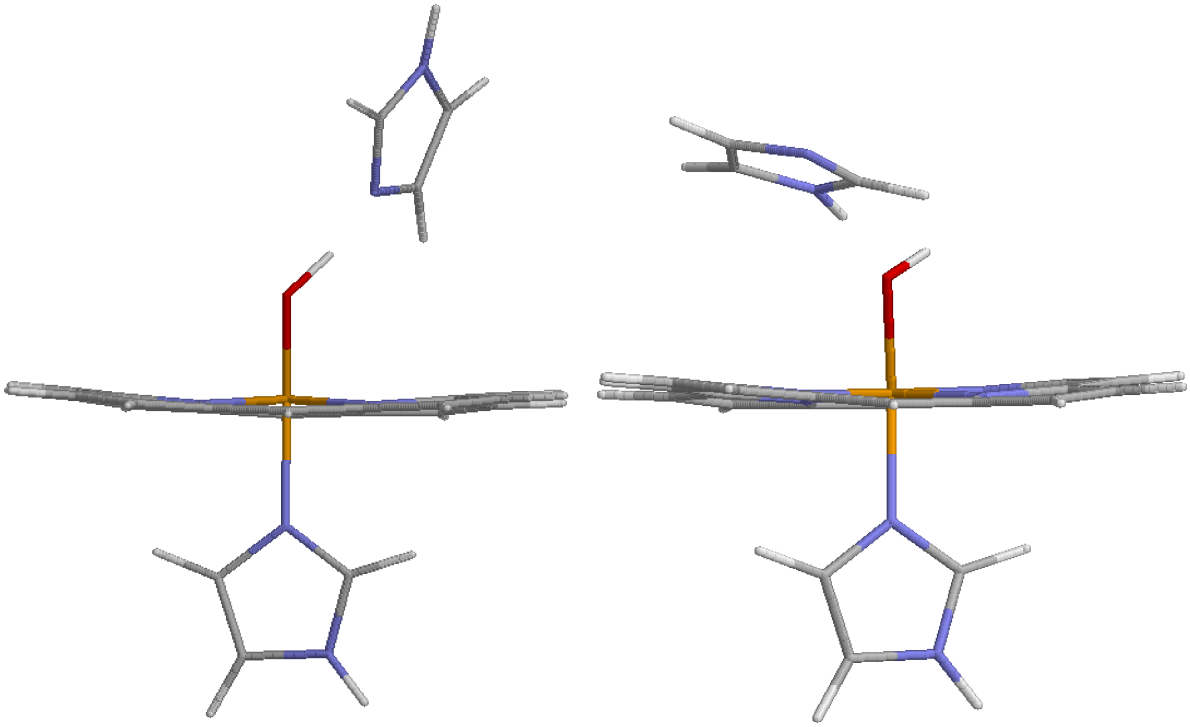

g h

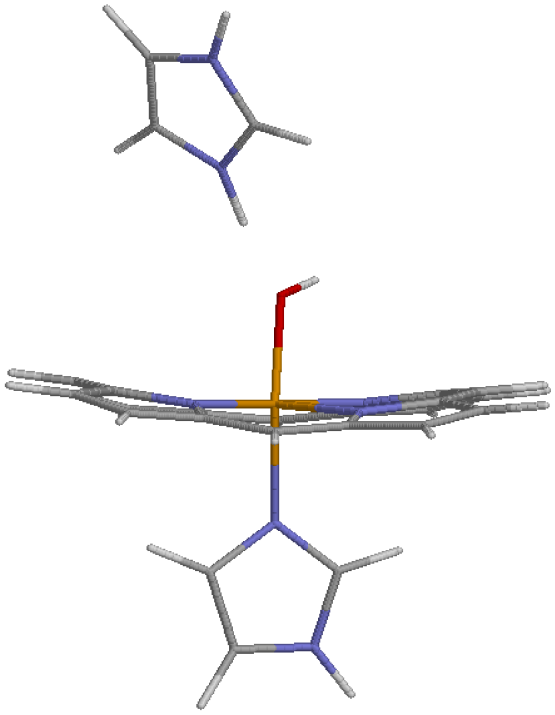

i

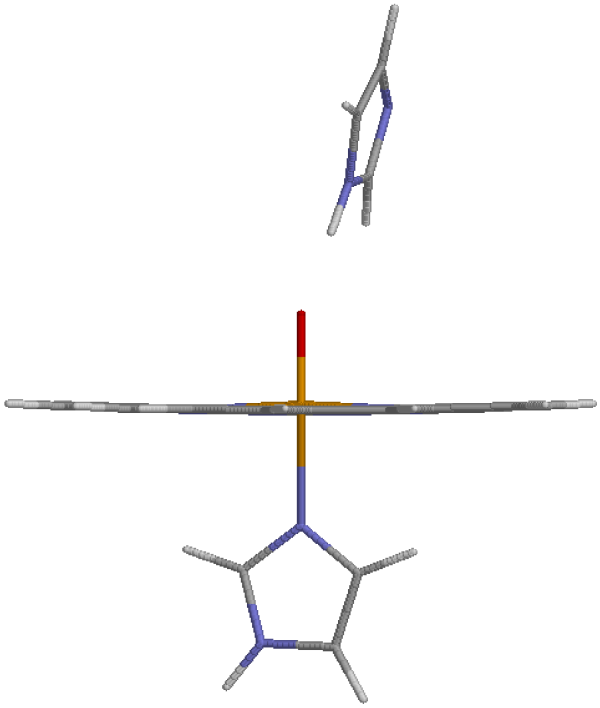

j

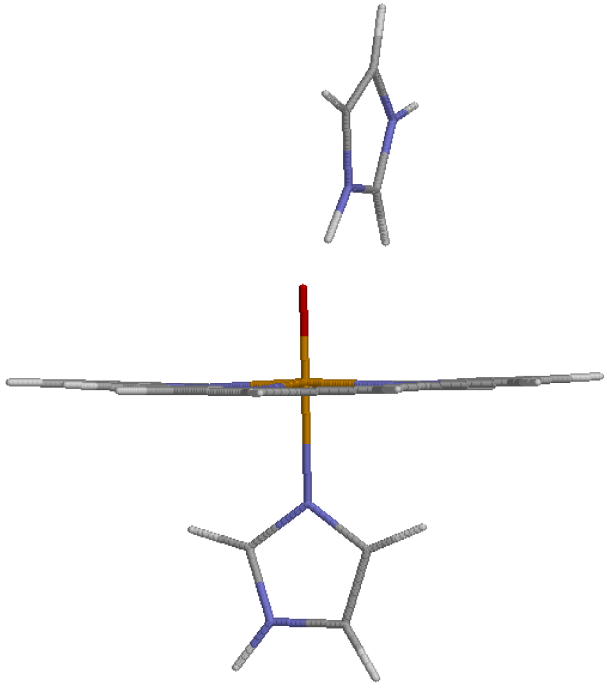

k

Figure 4. The three types of models of superoxide dismutase with (a) four, (b) five, and (c) six ligands, as exemplified by the Fe^{2+} complexes.

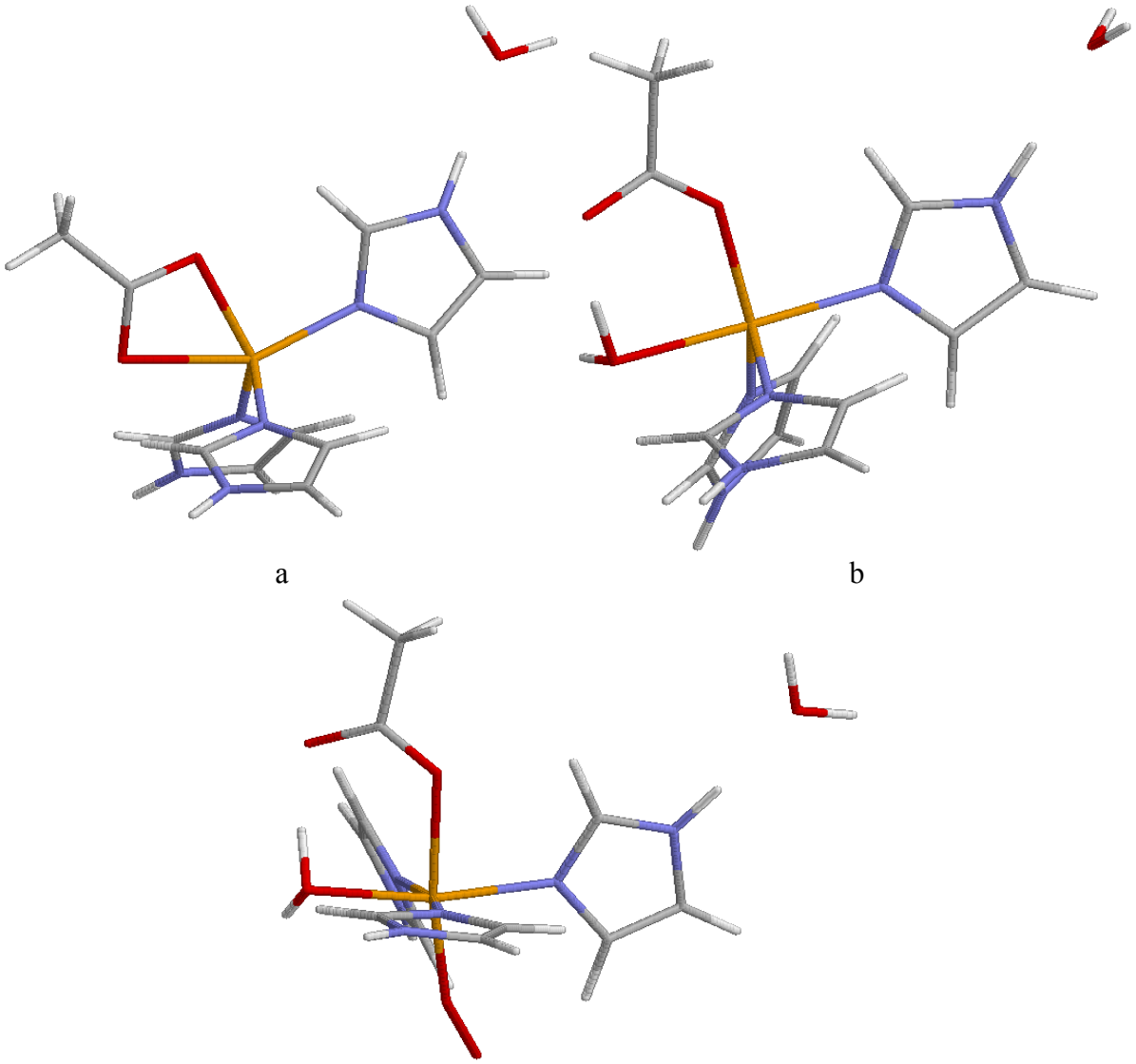

a b c

Figure 5. Iron–sulphur complexes with the water molecule forming one (a) or two (b) hydrogen bonds to the sulphur ligands.

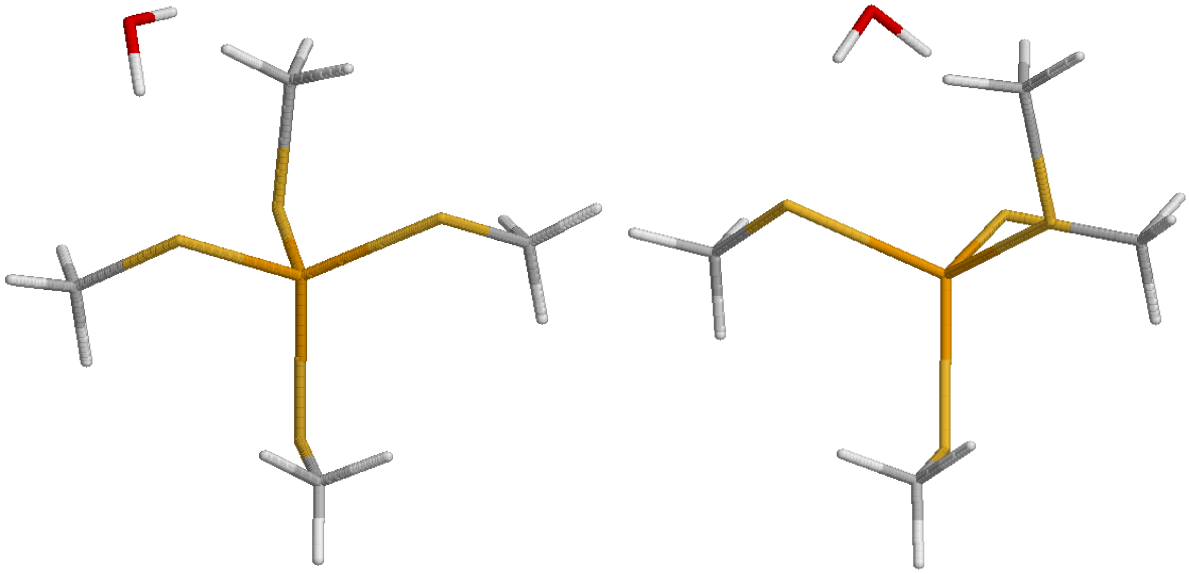

a b

Figure 6. The three carboxypeptidase models with water hydrogen bonding to the water (a), His (b), and Asp ligands (c).

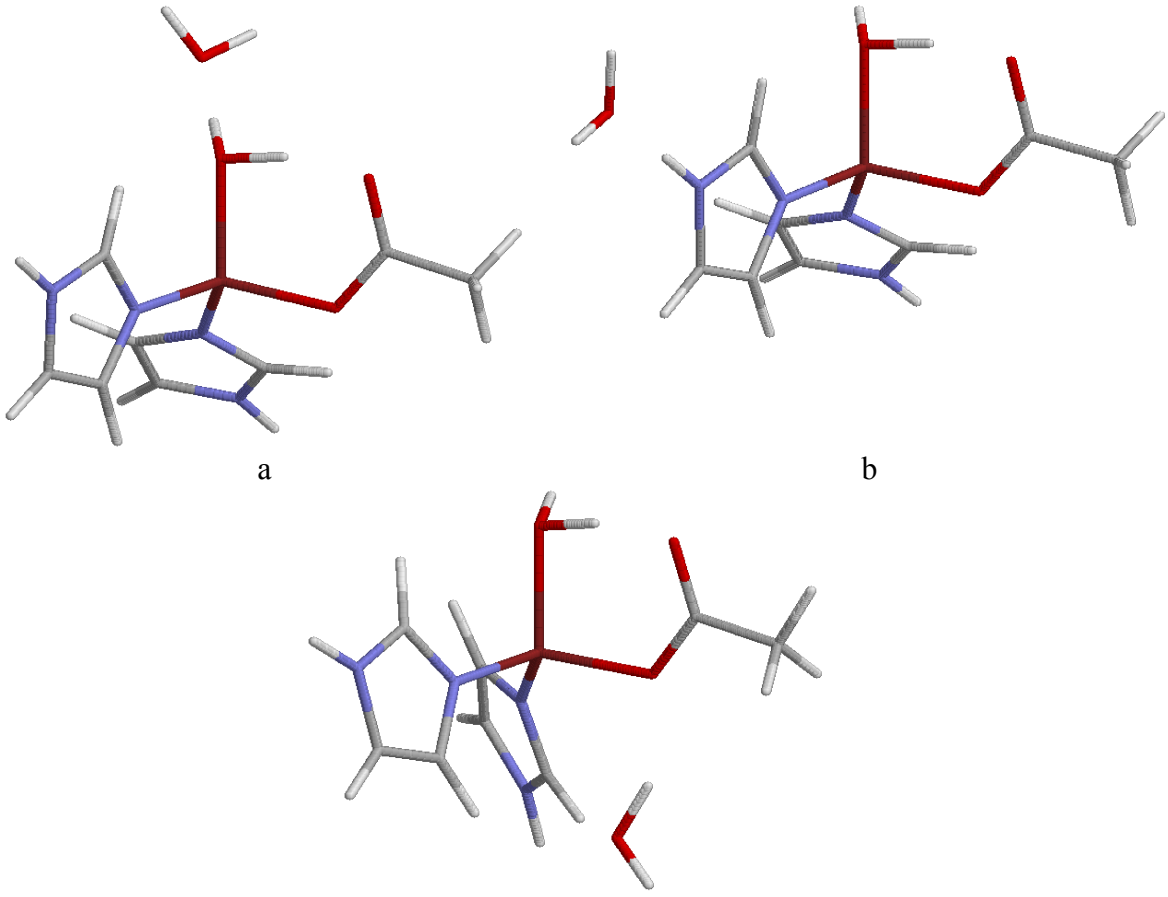

Figure 7. The five azurin models (here illustrated for the Cu^{2+} state) with a water molecule hydrogen-bonding to the two His ligands (a and b), the Cys ligand (c), the Met ligand (d), and the backbone carbonyl group (e).

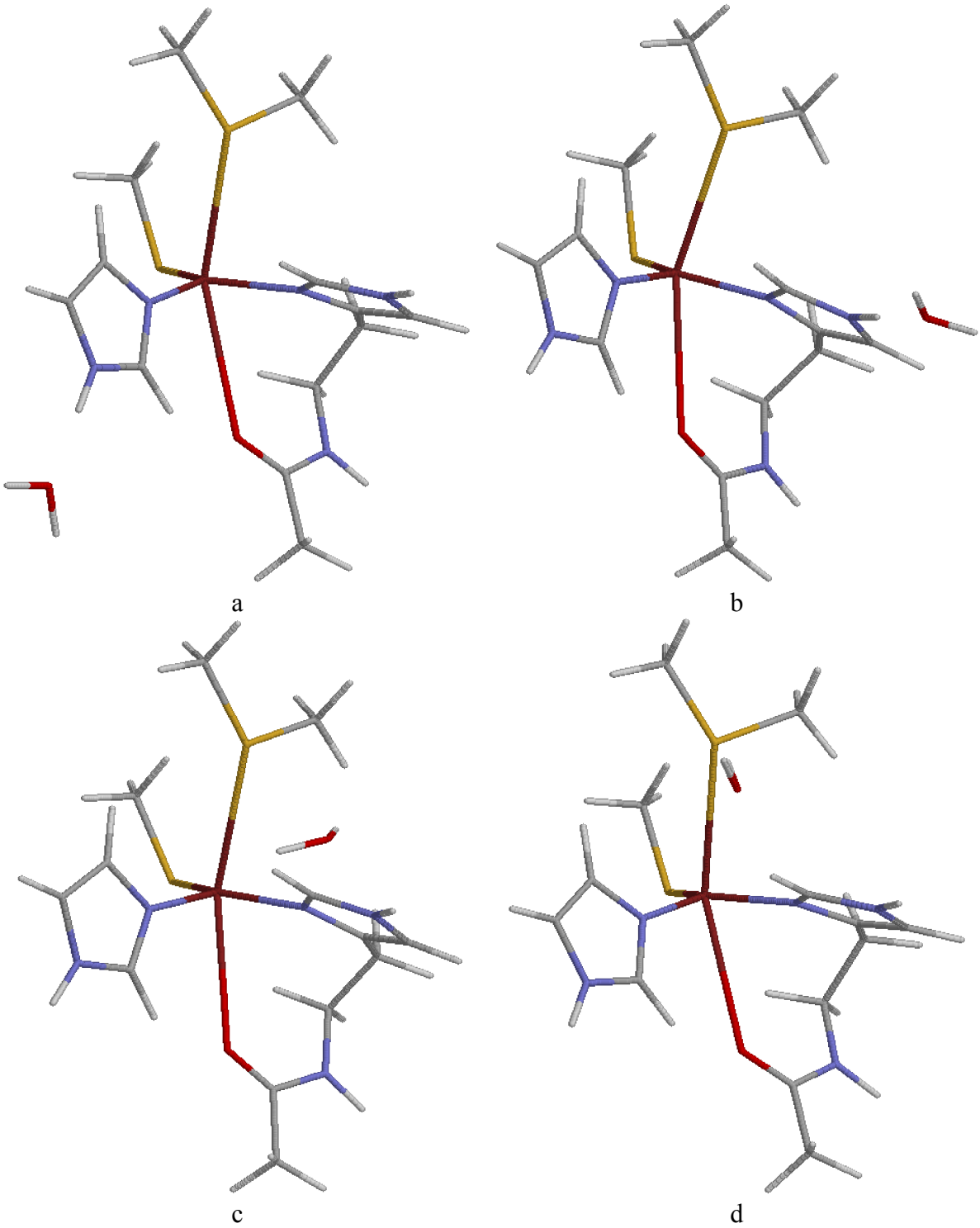

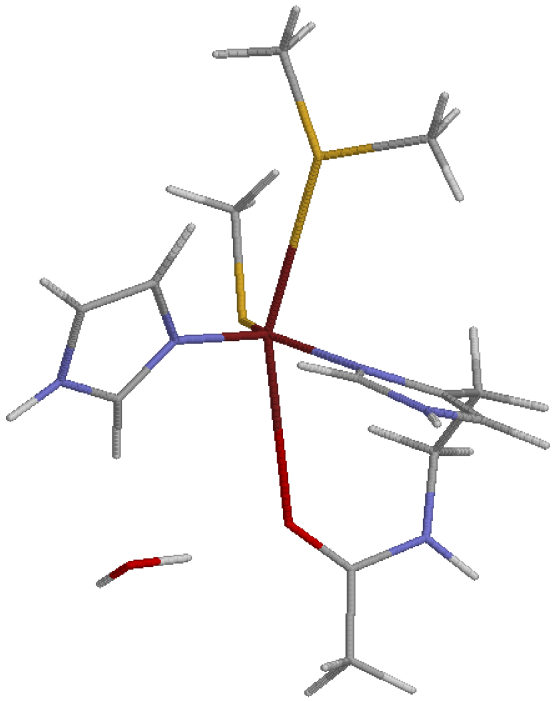

e

Figure 8. The five nitrite-reductase models with a water probe forming a hydrogen bond to the water (a) or OH^- ligand as an acceptor (b) or donor (c), or with an acetate probe forming a hydrogen bond to the OH^- ligand (d) or one of the imidazole ligands (e).

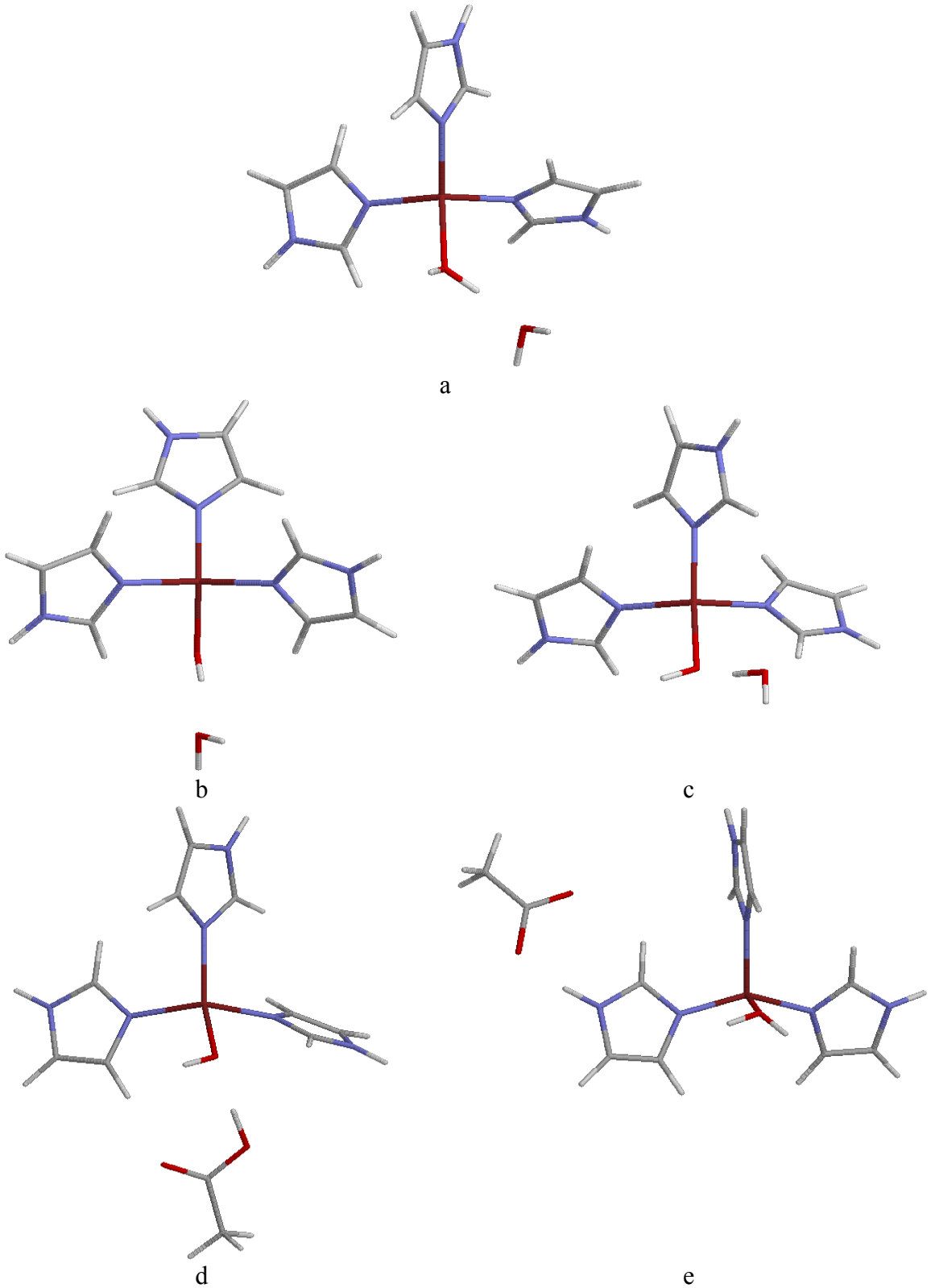

Figure 9. Hydrogen bonds to the propionate side chains of free porphyrin (a) and a desoxy

Fe^{2+} haem model (b).

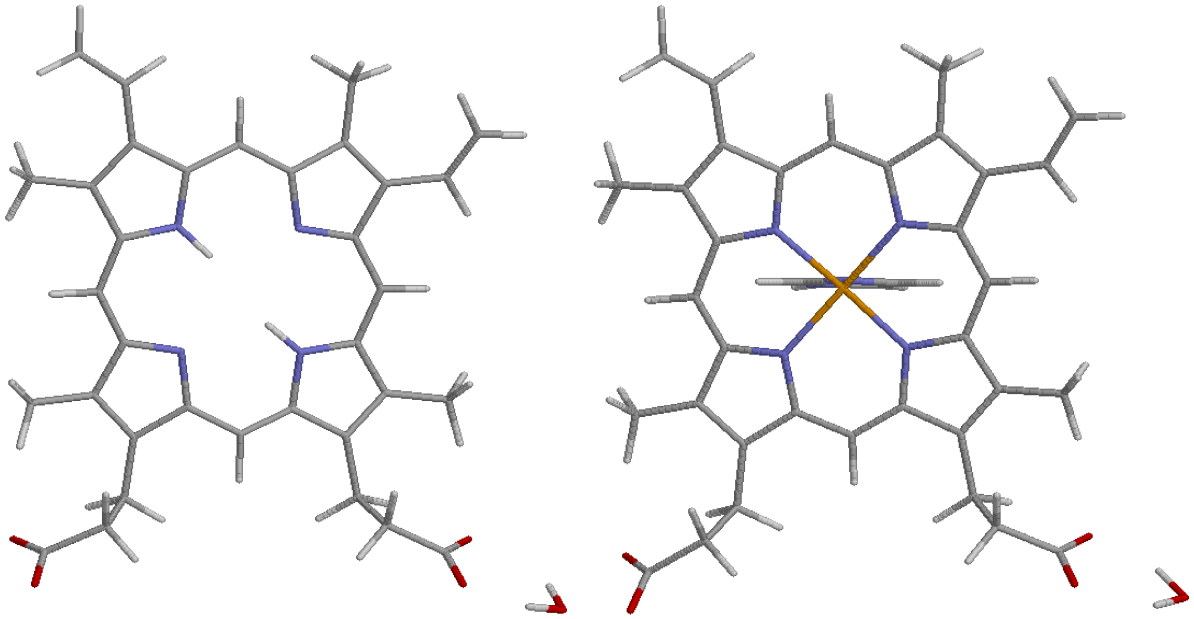

a b

Figure 10. Difference in hydrogen-bond energy between metal-bound and free ligands for systems involving a neutral (a) or negatively charged (b) ligand and a neutral probe molecule, calculated at three values of the dielectric constant and as a function of the net charge of the metal complex. A positive difference means that the metal complex has the stronger hydrogen bond.

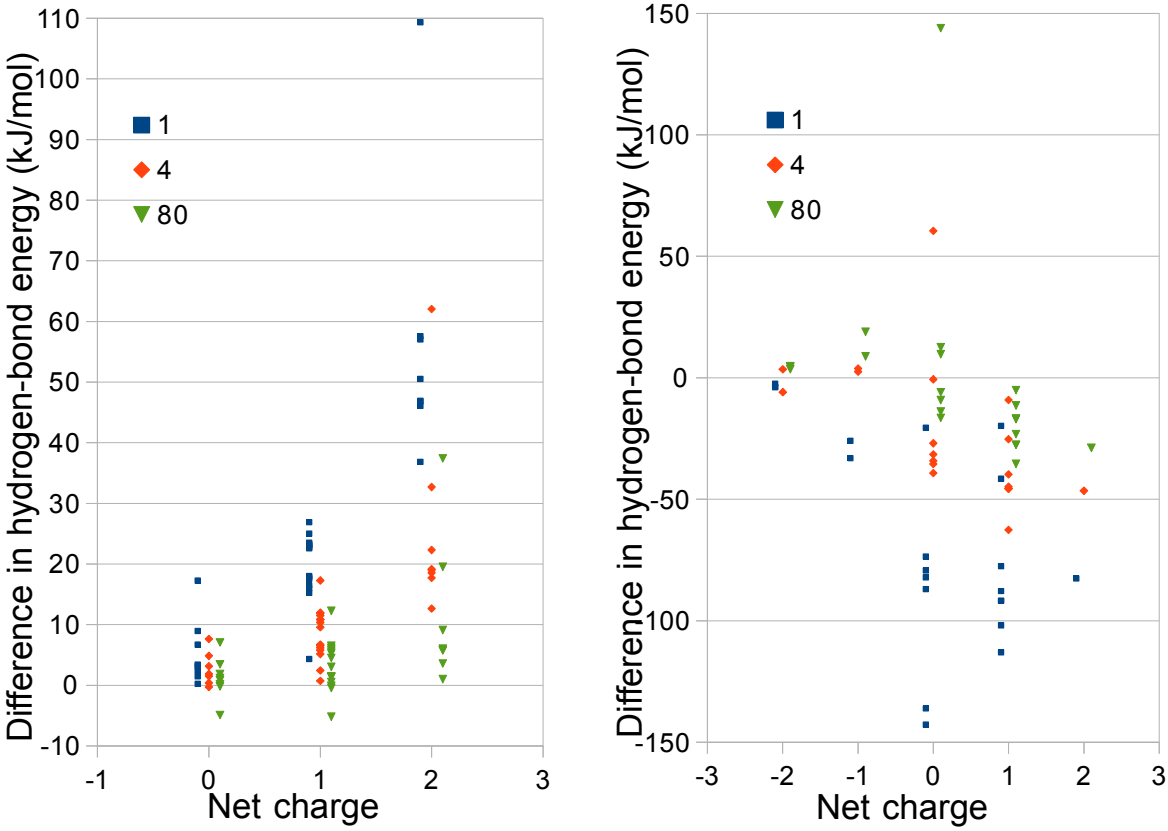

a b